IDENTIFICATION OF SITES FOR ARTIFICIAL GROUND WATER RECHARGE IN UPPER GANGA PLAINS, USING REMOTE SENSING – GIS

Project Final Completion Report

Funded by
Ministry of Water Resources, Govt. of India through INCOH

By

Dr. R. P. Gupta, Professor, Earth Sciences Deptt., IIT Roorkee

Dr. Sudhir Kumar, Scientist E2, NIH, Roorkee

Dr. A. K. Sen, Assoc. Professor, Earth Sciences Deptt., IIT Roorkee

DEPARTMENT OF EARTH SCIENCES

INDIAN INSTITUTE OF TECHNOLOGY ROORKEE
ROORKEE- 247 667

February 2011

Contents

List of Figures

List of Tables

IDENTIFICATION OF SITES FOR ARTIFICIAL GROUND WATER RECHARGE IN UPPER GANGA PLAINS, USING REMOTE SENSING – GIS

Project Completion Report   (per Appendix 5)

1. Name and address of the Institute

Name   INDIAN INSTITUTE OF TECHNOLOGY ROORKEE

Address   ROORKEE - 247667

Telephone: (Dean) 01332-285245   E-mail:<dsric@iitr.ernet.in>

Nearest Rail Head   ROORKEE

2. Name and address of the PI and other investigators

Name: Dr. R. P. Gupta (PI)

Designation: Professor

Address: Department of Earth Sciences, IIT Roorkee, Roorkee – 247 667

Telephone: 01332-285541   Fax: 01332-285638   E-mail: rpgesfes@iitr.ernet.in

Name: Dr. S. Kumar

Designation: Scientist E1

Address: National Institute of Hydrology, Roorkee – 247 667

Telephone: 01332-272906, Extn. 241   Fax: 01332-272123

E-mail: skumar@nih.ernet.in

Name: Dr. A.K.Sen

Designation: Assistant Professor

Address: Department of Earth Sciences, IIT Roorkee, Roorkee – 247 667

Telephone: 01332-285557   Fax: 01332-285638   Email: senakfes@iitr.ernet.in

3. Title of the scheme:

IDENTIFICATION OF SITES FOR ARTIFICIAL GROUND WATER RECHARGE IN UPPER GANGA PLAINS, USING REMOTE SENSING – GIS

4. Financial details:

Sanctioned cost: Rs.10,40,760/-

Amount released: Rs 7,65,000/

Expenditure: Rs. 7,06, 676/-

Unspent balance: Rs. 58,324/- adjusted as part payment towards Institute Infrastructure (Overhead Charges)

Return of unspent balance: NIL

Balance amount due:Rs. 1,15,136/- towards Institute Infrastructure (Overhead Charges)

5. Original objectives and methodology as in the proposal

■ *Application of Remote Sensing - GIS to map porous and permeable stretches of the palaeochannels which may act as sites for artificial recharge.*

■ *Study of the behaviour of groundwater table in the paleochannels vis-à-vis the adjacent terrain and trends of ground water flow.*

■ *Evaluation of hydraulic characteristics of the palaeochannel zone and the adjacent terrain.*

6. Any changes in the objectives during the operation of the scheme:

NIL; no changes were necessary

7. All data collected and used in the analysis with source of data.

The data used in this study can be broadly categorized into three main groups –

      (a) Remote sensing data,

      (b) Ancillary data, and

(c) Field data.

7.1 Remote Sensing Data

The study has mainly utilised remote sensing data from Indian Remote Sensing (IRS) satellite mission acquired from National Remote Sensing Agency (NRSA), Hyderabad, India. The IRS uses pushbroom scanning system based on Charge-Coupled Device (CCD), the sensors being called Linear Imaging Self Scanner (LISS-I and LISS-II). IRS-1B-LISS-II (www.nrsa.gov.in) data has been used for extracting information on geomorphology, vegetation cover, lineaments and paleochannel mapping in the research study.

It may be mentioned that the sensors LISS-II and LISS-III provide data in identical spectral bands, viz., green (0.52 - 0.59 µm), red (0.62 – 0.69 µm), and near-infrared (0.76 – 0.89 µm) bands, the difference being only in spatial resolutions (LISS-II = 36 m and LISS-III = 23 m). In this study, the objective is to delineate paleochannels which constitute regional/ major geomorphological features having dimensions of approx. 80 km length and 6-8 km width. For delineating such regional features, we have used LISS-II data (edge-enhanced with Laplacian isotropic filter) as good quality image data was available from this sensor. It is obvious that the use of LISS-III data would not have changed the interpretation.

Several remote sensing image data sets of different dates were acquired, processed and studied. In view of partial haze, cloud and other radiometric problems in image data sets, it was found that the multispectral image data set pertaining to the November 1998 gives the best results for landform mapping, land-use land-cover mapping and paleochannel delineation. Selected sensors specifications of this scene (IRS-1B-LISS-II) are given in Table 7.1.

7.2 Ancillary Data

A brief description of ancillary data, namely – topographic maps, soil maps collected from various sources and used in the study has been given in Table 7.2. Topographic sheets of Survey of India have been used for generation of base map of the study area. Various types of information e.g., contours and point elevations, drainage network and roads have been extracted from the topographic map. Soil map obtained

from National Bureau of Soil Survey and Land Use Planning (1999) has been used for obtaining information on soil characteristics of the study area.

7.3 Field Data

   Collection of field data is very important for any remote sensing and GIS based study. Extensive field work has been carried out during July 2004 to July 2007 for collecting various field data. The types and main purposes of field data collected from various sources have been given in Table 7.3. Field photographs and details of the field data have been incorporated at relevant places in subsequent sections.

Table 7.1: Salient characteristics of the satellite sensor data used.

Satellite/Sensor	IRS-1B, LISS-II
Date of acquisition	November, 1998
Path/Row	29-46B1
Spatial resolution	36.25 m
Quantization	8-bit
No. of bands	4
Spectral resolution	Band1 (Blue) : 0.46-0.52μm Band2 (Green) : 0.52-0.59μm Band3 (Red) : 0.62-0.68μm Band4(NIR) : 0.77-0.86μm
Swath width	74 km
Format	Band Interleaved by Line (BIL)
Repeat Cycle	22 days

Table 7.2: Ancillary data used in this study.

Data type	Specification	Source
Topographic Maps	Scale 1: 50,000 (Toposheet Nos. 53G/9, 53G/13, 53G/14, 53G/15, 53K/1, 53K/2, 53K/3)	Survey of India, Dehradun
Soil Map	Scale 1: 500,000 (Sheet No.1; Soil Map of Uttar Pradesh)	National Bureau of Soil Survey and Land Use Planning (ICAR), 1999
Other Data (soil texture, specific yield, storage coefficient etc.)	----	Groundwater Division Uttar Pradesh and various published Journals, reports and maps

Table 7.3: Field data types and their purposes.

Data type	Purposes	Source
Litholog data	To construct aquifer geometry, and to estimate vertical hydraulic conductivity	Tube Well Division of Uttar Pradesh Dedicated field drilling operation
GPS data (Differential GPS)	To determine latitudes, longitudes and ground height (from mean sea level) of water level recording stations where ground levels were not available	Hand held GPS survey Differential GPS survey
Groundwater level data	To estimate unsaturated aquifer thickness and ground water flow direction	Groundwater Division Uttar Pradesh Water level monitoring programme
Rainfall data	To estimate surface runoff and recharge rate	Groundwater Division Uttar Pradesh

Tracer data (Tritium injection)	To find out recharge rate and specific yield	Dedicated field work
Ground water sample	To obtain information on recharge source through stable isotope analysis	Dedicated field work
Soil samples	To obtain soil textural information	Dedicated field work

(a) Litholog Data Collection

The litholog data are used for constructing aquifer geometry and to estimate vertical hydraulic conductivity of both paleochannel and adjacent aquifer. The details about the litholog data are described below:

Collection of Existing Lithologs: A large number (more than 100) of vertical bores have been drilled by the Tube Well Division of Uttar Pradesh (earlier including the present Uttarakhand state also) in the study area. Well-log data of these bore wells are available in the form of tables, representing depth of strata below ground level, strata numbers, nature and thickness of strata, along with village/location name. Selected well-logs pertaining to the study area have been collected from the Tube Well Division of Hardwar (Uttarakhand), Saharanpur and Muzzaffarnagar (U. P).

Drilling Operations: Most of the bore logs collected from the Tuble Well Division of Uttar Pradesh pertain to non-paleochannel area. They also have a large variation in strata penetrated, level of details, and lithological description. Therefore, some boreholes were drilled both on the paleochannel and the alluvial plains to fill up gaps and also to check the collected lithologs with respect to the drilling observations. Sampling has been carried out for collecting lithological information at different depths in the boreholes drilled. Firstly, paleochannels have been mapped from remote sensing data analysis. These paleochannels have been traced and displayed on the base map by GIS and sites are selected systematically for drilling. A series of 17 wells systematically sited on the paleochannel and the alluvial plains have been drilled (for location sites see Figure 8.8).

14

Both shallow (depth upto 20 m) and deep (depth upto 80 m) bore wells were constructed by 'Bukki' method (Figure 7.1 a & b). Lithologs are given in & Figures 7.2-7.5.

(b) Soil Sample Collection

Soil samples were collected from different types of land use, using hand auger from a depth ranging up to 50 cm and stored in clean self-sealing plastic bags before transportation from the sits. The soil samples were air-dried in the laboratory, and passed through a 2 mm sieve, after they had been disaggregated with a porcelain pestle and mortar. Subsequently, samples were stored in clean self-sealing plastic bags for further analysis.

(c) Laboratory Analysis of Soil Samples

Soil texture is a term commonly used to designate the proportionate distribution of different sizes of mineral particles in a soil. It dose not include any organic matter (Brown, 1990). Preparation of the samples for textural analysis consisted of the following steps (Carver, 1971):

(i)   Breaking all clumps and mashing with fingers.

(ii) Mixing sample thoroughly and splitting.

(iii) Coning and Quartering the sample.

(iv) Taking 50-100 gm sample chunk, removing carbonates by adding in1N HCl with stirrer and rim washing, followed by decanting HCI.

(v) Removing organic matter by adding 6% to 30% H_2O_2, stirring and rim washing.

(vi) Adding distilled water and heating on hot plate for 12 hours (at 40°C temperature).

(vii) Removing Iron Oxide by adding distilled water, aluminium foil and 15 gm Oxalic acid with stirrer and heating on hot plate for 10 to 25 minutes followed by decanting excess clear water.

(viii) Drying and weighing.

(d) Groundwater Level Monitoring

Groundwater level data forms mandatory parameters in artificial groundwater recharge study. The zone of deeper water levels indicates maximum thickness of unsaturated zone and hence forms suitable sites for artificial recharge. Also water level data analysis along with other factors is of great importance to analysis the necessity of artificial recharge over the study area. During the feasibility study, the monitoring of groundwater level greatly help in identifying the method of artificial recharge. The depth of water table at post monsoon period is vital for estimating the thickness available for recharge. Ground water flow direction map is helpful because it determines whether the groundwater will flow away from the location where it is recharges artificially or not. If the groundwater flow direction is away from the location where it is recharged artificially, more water can be added / supplied for recharge. Hence, those sites are very important for artificial recharge.

Groundwater levels have been monitored at 37 locations (12 on the paleochannel aquifers and 25 on the adjacent alluvial plains aquifer) over 2 years (2005-2006) for both pre- and post-monsoon period. Some key wells were also monitored in the subsequent year (2008). The precise locations (x, y, z co-ordinates) have been determined through differential GPS. Groundwater levels were measured using a survey-grade groundwater level indicator.

(e) Tracer (tritium) Investigation

Estimation of infiltration rate or the recharge rate helps to design suitable artificial recharge structures and to assess the extent of recharge from these structures. Areas with high infiltration/recharge rate are more suitable for artificial recharge. So, it is very much essential for estimating recharge rate/infiltration rate for artificial groundwater recharge studies. Here, recharge rate due to precipitation have been estimated using tritium tagging technique along with remote sensing and rainfall data. The technique of estimation of recharge rate by using artificial tritium method was first applied by Zimmerman et al. (1967 a, b) in West Germany. The basic principle of this technique assumes that the soil water in the unsaturated zone moves downward "layer by layer" similar to a piston flow.

Since the lateral molecular diffusion mixes the percolating water rather fast, this assumption is probably valid in most natural situations e.g. in the alluvial formations, except where the alluvial cover is too thin and the basement rock is at a shallow depth or where the" fissures and/or discontinuities are present in the soil profile (NIH,1986 and 2000). On the basis of this assumption, if fresh water tagged with tritium enters the top of the soil below the active root zone, and is not affected by evaporation, the tagged tritium will be mixed with the soil moisture available at that depth and act as an impermeable sheet. In this case, if any water is further added at the top of the soil surface, it will be infiltrated into the ground by pushing down the older water, thus the shift in the tritium peak can be observed after some time (say after lapse of one season). Recharge rate has been calculated from the tritium peak shift, rainfall and grain size analysis**.

8. Methodology-Overview

The broad methodology adopted in the present study has been outlined in Figure 8.1. Details of methodologies employed in the procurement and analysis of the different data sets have been discussed separately at relevant places in the succeeding chapters.

In this work, particular emphasis has been placed on using remote sensing – GIS technology for the study aimed artificial groundwater recharge in the area. The entire study has been carried out in GIS environment. A base map has been prepared by scanning, geo-referencing, mosaicking and digitizing the Survey of India (SOI) topographic maps. The various data layers have been co-registered with the base map. Point data obtained from field and laboratory experiment are properly placed on the base map and finally various information have been obtained using GIS tools.

Software Used

The remote sensing data has been processed by using ERDAS Imagine-8.7 software. The GIS analysis has been carried out using ILWIS-3.3, ARCVIEW-3.2 and R2V software. Litholog data analysis is carried out by using ROCKWORKS-2006 software.

8.1 Mapping of Major Paleochannels from Remote Sensing Data

In this study, the major emphasis is on artificial groundwater recharge, for which in the first stage site selection is required. The study area is a part of the Indo-Gangetic plains and is quite devoid of any significant relief features and physiographically exhibits the typical characteristics of a river flood plain. The various major physiographic/landform units are – (a) vast stretches of alluvial plains, (b) dry streams, (c) paleochannels, and (d) marshy land (Kumar et al., 1996; Sammdder et al., 2007). The river paleochannel deposits are significantly different from the vast alluvial deposits being composed of coarse sand with pebbles, boulder, cobbles etc. and have been came from well developed regionally extensive earlier river systems. The landcover types are closely related to the landform units. Therefore, as a first step, landcover/landform mapping has been carried out using remote sensing data.

8.1.1 Major Landform/Landcover (LULC) Classes

Due to synoptic view, map like format and repetitive coverage, satellite remote sensing imagery is a viable source of gathering quality LULC information at local, regional and global scales (Csaplovics, 1998; Foody, 2002; Gupta, 2003). In this study, six LULC classes have been identified. These are – agricultural land, paleochannel, dry streams, water body, built-up area, and marshy land. Pre-processing and processing of remote sensing data has been discussed in the subsequent section to follow. Detailed characteristics of all the classes along with their interpretative characteristics on each band as well as on the colour infrared composite of LISS-II image are given in Figure 8.2, Figure 8.3, and Table 8.1

8.1.2 Pre-Processing of Remote Sensing Data

A digital image is a two-dimensional data array of brightness values representing spectral response of the scene captured. It typically comprises of small equal-sized areas called pixels (picture elements), which form the ground resolution cell. A digital image often contains distortions with respect to its geometry and radiometry (e.g., atmospheric

effects). Therefore, the data needs to be pre-processed to rectify for various distortions. The rectified image is then subjected to a number of image processing operations, such as contrast enhancement, image ratioing, classification, etc. for extracting useful information related to the Earth's environment. An overall framework of various digital image processing operations adopted here for various task is shown in Figure 8.4.

(a) Geometric Correction

The digital images acquired from remote sensing satellites are fraught with geometric distortions, which render them unusable, as these may not be directly correlated to ground locations (Gupta, 2003). The geometric distortions in images may occur due to several reasons, such as Earth's curvature, panoramic distortion, etc. Geometric correction involves the process of assigning map coordinate information to the image data so that the geometric integrity of the map in the image is achieved.

Table 8.1: **Characteristics of landcover/landuse classes.**

Landcover classes	Description	Blue Component Green Band	Green Component Red band	Red Component NIR band	CIR composite
Agricultural Land	Sparse vegetation, agricultural activity	Dark	Very dark	Medium to dark	Dull red
Water body	River, Ponds etc.	Light	Light	dark	Cyanish blue to Blue
Paleochannel	Very low vegetation density,	Grey	Light	light	Yallowish -white

	agricultural activity, fallow land				
Marshy land	Low lying land stagnant with shallow depth water throught the year	Very dark	Very dark	Medium to dark	Black
Built-up area	Town and villages; block like appeaence	Light grey	Grey	Darker	Bluish grey
Dry stream/flood plains	Dry sand appear in the bank of river	Dark gray	Dark	Dark	Cyanish-white

Geo-referencing is commonly performed using the method of rubber-sheet stretching that has been explained in many standard texts (e.g., Mather, 1999; Gupta, 2003). A number of ground control points (GCPs) distributed uniformly over the entire area are collected such that they can be easily located on both the image to be rectified and the reference map, such as a toposheet. A GPS survey is often carried out for accurate determination of coordinates of the GCPs.

In this study, the geometric correction of remote sensing data (IRS-1B-LISS-II image) using the above procedure has been performed on ERDAS Imagine. In the first step, Survey of India toposheets (53G/9, 53G/13, 53G/14, 53G/15,53K/1, 53K/2, 53K/3 at 1: 50,000 scale) have been scanned to convert the paper maps into digital format. The scanned toposheets have been geo-coded using the latitude and longitude information of the graticule intersections and reprojected to Polyconic projection system with Everest

1956 spheroid and India-Nepal as datum (Table 8.2). A mosaic of these geo-coded toposheets has been generated and used as reference map or "master" for geometric rectification of satellite images and geological maps.

Table 8.2: Properties of map projection system used.

Projection	Polyconic
Spheroid	Everest 1956
Datum	India-Nepal
Longitude of Central Meridian	$77^0 44^{'} 59.32^{''}$E
Latitude of Origin	$29^0 45^{'} 0.13^{''}$N
False Easting	5,00,000.0
False Northing	5,00,000.0

Remote sensing data (IRS-1B-LISS-II) have been geo-referenced with reference to the base or master map by taking input GCPs from LISS-II image and the reference GCPs from topographic (master) map. A large number of well distributed points (like intersection of roads, road and canals, bifurcation of canal etc.) identified both on the image and the reference map have been taken as GCPs in view of the absence of other distinct features in the area.

As this is a plain area, eighteen GCPs are found to be enough for adequate geometric correction of remote sensing data. A Root Mean Square (RMS) control point error of 0.252 pixel has been obtained by using 2nd order polynomial model, which is well within the acceptable limit of one pixel for such type of study. The nearest-neighbour resampling method has been adopted to generate the final geo-referenced LISS-II image, as this preserves the original brightness values in the output image.

(b) Radiometric Correction

The optical remote sensing data invariably contains the atmospheric haze components due to atmospheric interaction. In the visible – near infrared region of the

21

electromagnetic spectrum, scattering is the most dominant process leading path radiance. This has an additive role and affects the brightness values (Jensen, 1996). The remote sensing data, therefore, need to be corrected for removing atmospheric haze components. Although there are many techniques to perform this correction, the most widely used 'dark-object subtraction' technique (Chavez, 1988) has been adopted here to correct such atmospheric haze effect. This is a simple, fast to implement, empirical procedure. The method is based on the assumption that in every image there should be at least a few pixels completely dark (0% reflectance); they may correspond to areas of deep, clear, open water bodies, deep shadows etc. Ideally, these pixels should have DN values of zero; however, because of the atmospheric haze, they record non-zero values. This characteristic is used in empirically for estimating the haze component. In practice, the method involves first locating clear, open and deep water bodies or completely shadowed (dark) areas (where ground reflectance can be considered to be null and the DN-values in infrared channels are also generally nearly zero). The minimum DN-value in each channel over such pixels is taken as the path radiance and is subtracted from all other pixel values in the respective channel.

(c) Noise Removal

An efficient method to remove noise from digital image is through Fourier analysis. Strippings are seen on the LISS image, which have been removed through Fourier filtering. Initially, First Fourier Transformation is calculated which gives the Fourier spectrum of the raw image. The Fourier spectrum shows the different anomalous high frequencies that are responsible for different type of noises. So, initially a low pass filter is applied on the image to block the high frequencies. The corresponding IFT (Inverse Fourier Transform) is calculated. Then the wedge filter is applied in the direction of the axis and the abnormal patches in the spectrum are blocked by using symmetrical rectangular and circular filters. These filters are used carefully because application of such filtering may block certain important frequencies which may results in complete black-out of the image. Application of wedge filters and corresponding transformation through IFT gives an image where the noises are removed.

(d) Image Enhancement

The purpose of image data enhancement is to render the set of digital image data more interpretable. Various standard digital image processing techniques can be applied to remote sensing data to extract information on geology, geomorphology, land use, structural features and vegetation cover (Jensen, 1996; Gupta, 2003). In this study, the following types of image enhancement techniques have been applied on rectified LISS-II image:

Edge Enhancement and Linear Contrast Stretching: Individual spectral bands have been edge enhanced to emphasize high frequency variations and subsequently these enhanced bands have been used to generate Colour Infra-red composite (CIR composite). Various features like transport network, boundaries of water bodies, paleochannel boundaries etc. get very distinct on edge enhanced image. In the present case, edge enhancement followed by linear contrast stretching of individual bands of LISS-II data set have been applied for improving interpretability.

CIR composite : As the near infrared band gives information on surface moisture and the red band on vegetation, further interpretability is improved by making CIR composite using the enhanced NIR, Red, and Green bands (coded in red, green and blue colour respectively) (Figure 8.3).

8.1.3 Processing of Remote Sensing Data

(a) Image Classification

A classification scheme defines the number of LULC classes to be considered to perform remote sensing image classification. Sometimes, a standard classification scheme, such as Anderson's LULC classification system (Anderson et al., 1976) may be used, while at other times the number of LULC classes may be chosen according to the requirements of the specific project for a particular application. In this study, six LULC classes have been chosen (Table 8.1) Supervised classification scheme is applied for generating LULC map over the study area using - (a) LISS-II Colour Infra-red composite (base map), and (b) field data (ground truth). The preparation of reference data has been ably supported

with field surveys and previous knowledge of the study area. The GPS survey has been carried out to obtain accurate location of LULC classes for their easy demarcation on geo-rectified LISS-II image. All the processing steps have been implemented in ERDAS Imagine and ILWIS software.

The classification has been performed using the most widely used Maximum Likelihood Classifier (MLC) (Figure 8.5). The MLC assumes that spectral values of the training pixels are statistically distributed according to a multi-variate normal probability density function. For each set of spectral input values, the distance towards each class mean is calculated using Mahalanobis distance. The algorithm for calculating the distance to class means is

$$D_i(x) = \ln |V_i| + y^T V_i^{-1} y$$

Where, D_i = Distance between spectral input x and class mean based on probabilities

x = Spectral input (feature vector)

y = Distance towards a class mean.

y^T = Transpose of y

V_i = M × M variance-covariance matrix of a class, M is number of bands

$|V_i|$ = Determinant of V_i

The distance to class means thus computed is used to define the class name of the input pixel. The class name with the shortest distance to mean is assigned to the input pixel if this distance is smaller than a user defined threshold value; else an undefined value is assigned.

(b) Post-Classification Filtering

Some stray pixels always occur in a LULC classification produced from remote sensing data. To remove these stray pixels and to generate a smooth image, a 3 × 3 pixels majority filter has been applied, which assigns the most dominant class to the central pixel (Figure 8.6). An error matrix has also been prepared for the accuracy assessment of the classified image (Table 8.3).

Table 8.3: Error matrix of the classified image obtained from classification of data with 1, 2, 3, 4 band combinations of LISS-II data.

Classes in the classified image	Classes on reference data						
	1	2	3	4	5	6	Row total
1. Agriculture	**189**	0	0	1	6	1	197
2. Settlements	0	**128**	7	3	0	0	138
3. Water body	2	24	**147**	0	0	2	175
4. Dry streams	1	0	1	**132**	35	0	169
5. Paleochannel	3	0	0	28	**185**	0	216
6. Marshy land	1	8	0	1	0	**123**	133
Column total	196	160	155	165	226	126	**1028/1028**

8.1.4 Paleochannel Mapping

Finally, integrating information from CIR composites, LULC map, and extensive field observations, paleochannels have been traced and a paleochannel map has been generated (Figure 8.7). The existence of paleochannels has also been cross-checked from litholog data and field observations. It has been observed from field observation that in the northern upper part, paleochannels are suddenly cut by one fault-scarp (Figure 8.3, Figure 8.2c). The fault-scarp appears as narrow zones having similar signature like paleochannel. The south-western side of the fault-scarp is up-thrown and north-eastern side is down-thrown. The ground height difference between up-thrown and down-thrown is about 5 m. So, for preparation of paleochannel map, this falt-scrap is also taken into consideration.

8.1.5 Distribution of Major Paleochannels

In the study area, three major paleochannels exhibiting broadly successive shifting and meandering pattern have been deciphered (Figure 8.7). Some of the

paleochannels when extended northwards meet the point, where the Yamuna and Ganga rivers debouch from the Siwalik Hills, into the plains, indicating that these rivers were active on this unit in the past, which is upland in nature presently. The characteristics of the major paleochannels over the study area are described below:

Paleochannel 1: It runs from east of Purkaji to near Chappar and then turns westward upto Muzzaffarnagar (marked as P1 in Figure 8.7). The trend of this paleochannel is NNE-SSW. The width varies from 2.3 km to 3.8 km, average being 3.0 km. The length is about 35 km. The areal extent is 105 square km.

Paleochannel 2: The second main paleochannel (marked as P2 in Figure 8.7) starts from near Baseri village through Quasimpur upto Jatwara. The average width of this paleochannel is 3.2 km. The length is about 30 km and the areal extent is 103.5 square km.

Paleochannel 3 (marked as P3 in Figure 8.7): This paleochannel starts from Sukratal through Mirahpur and extends southward parallel to the Ganga river upto Hastinapur. The width of the paleochannel is about 4.2 km. The length is more than 40 km.

All of these paleochannels in this study area are broadly N–S trending and are located to the west of the present day course of the river Ganga. So, it can be inferred that the Ganga River has been shifted successively from the west to the east. Most of the paleochannels are very wide (2-5 km) suggesting their formation by large river. A field work to the area has been carried out. It has been found during the field observation that the soils on the paleochannels are coarse sand or at times it appears pure sand (Figure 8.2a). Scant agricultural activity and mostly devoid of vegetation on the paleochannels are indicative of high permeable, porous, coarse grained materials possessing high infiltration rate.

8.2 Hydrogeological Characteristics

In the foregoing section, we have presented the results of landform mapping in the area. It has been shown that the area comprises of dominantly vast stretches of alluvial

plains within which there are major paleochannels. From the point of view of artificial recharge of groundwater, the paleochannels hold distinct promise. Therefore, it is important to study the hydrogeologic characteristics of both the landforms, viz. the paleochannels and the adjacent alluvial plains, their recharge rate and hydrogeologic mutual interconnectivity, groundwater flow pattern, recharge sources, rainfall runoff etc., in order to assess the suitability of these units for artificial groundwater recharge.

In this section, first, the results of soil texture analysis are given which describe the compositional characteristics of the soils of the two landform regions. This is followed by results of computed vertical hydraulic conductivity values based on soil texture data. Then, the present-day recharge sources of groundwater are discussed. Finally, based on groundwater level data, groundwater flow analysis is presented.

8.2.1 Soil Texture

Tweenty (20) surface soil samples, collected from sites located on both the paleochannels and alluvial plains, have been subjected to grain size analysis to yield information on soil texture. From the mechanical analysis of soil samples in the laboratory, the percentage for each of the soil fractions (sand, silt and clay) were determined. The percent of each the soil fractions (sand, silt and clay) are plotted on the USDA textural triangle (Brown, 1990; Bouwer, 2002). From this plot, textural class of the soil sample were determined. The location map of soil samples is given in Figure 8.8. The triangular plot is shown in Figure 8.9 and the overall summary of grain size analysis is given in Table 8.4 and Table 8.5.

From this soil textural analysis, the following observations have been made:
(a) It has been observed that in the area of paleochannels, the percentage of sand varies from 58.3 to 78.6 and that of silt and clay varies between 7.0 to 29.1 and 7.3 to 16.3 respectively. On the other hand, in the areas of alluvial plains, the sand percent varies between 15.1 to 28.8, whereas silt and clay percentage is between 51.9 to 69.3 and 11.8 to 24.2 respectively.
(b) This shows that the paleochannels comprise dominantly sandy loam type of soil, on the other hand, the alluvial plains are characterised by silty loam type of soil (Figure 8.9, Table 8.4, Table 8.5).

8.2.2 Vertical Hydraulic Conductivity

A series of 17 observation wells systematically sited on the paleochannel and its either flanks have been drilled (Figure 8.8) and sampling has been carried out for collecting lithological information at different depths. Grain size analysis has been carried out for all the 82 samples collected from different locations and at various depths during drilling. The grain size distributions have been plotted on lognormal graph paper to obtain grading curve for each sample. D_{10} has been calculated for each sample form the grading curve and subsequently bulk hydraulic conductivity has been determined using Hazen (1911) equation. The D_{10} is the grain size (in millimeters) at which 10 percent by weight of the sample has been retained and 90 percent of the sample has passed. The Hazen approximation was used to estimate bulk hydraulic conductivity where the D_{10} is

Table 8.4: **Sand, silt and clay percent of soil samples falling in paleochannel.**

Location Name	Sand%	Silt%	Clay%
S1	72.5	11.2	16.3
S2	67	18.3	14.7
S3	68.2	24.4	7.4
S4	58.3	29.1	12.6
S5	75.1	9.8	15.1
S6	78.5	7	14.5
S7	73.6	19.1	7.3
S8	71.11	16.29	12.6
S9	76	13.75	10.25
S10	78.6	7.8	13.6

Table 8.5: Sand, silt and clay percent of soil samples falling in alluvial plains.

Location Name	Sand%	Silt%	Clay%
S11	20.5	55.3	24.2
S12	26	52.5	21.5
S13	22.3	61.4	16.3
S14	15.1	69.3	15.6
S15	28.8	54.7	16.5
S16	18.3	63.2	18.5
S17	21.7	66.5	11.8
S18	20.7	58.5	20.8
S19	28.6	51.9	19.5
S20	24.2	62.2	13.6

Table 8.6: Values for the coefficient 'C' (Fetter, 1994).

Soil characteristics	Values of C
Very fine sand, poorly sorted	40–80
Fine sand with appreciable fines	40–80
Medium sand, well-sorted	80–120
Coarse sand, poorly sorted	80–120
Coarse sand, well sorted, clean	120–150

between 0.1 and 0.3 mm (Hazen, 1911; Fetter, 1994). The Hazen (1911) equation is as follow:

$$K = C\,(D_{10})^2$$

Where, K is bulk hydraulic conductivity (centimeters per second) and C is a coefficient assigned to the sample based on the characteristics of the D_{10} (centimeters). The Table 8.6 shows values for the coefficient C.

The grading curves for different samples are shown in Figure 8.10 and Figure 8.11. The estimated D_{10} and bulk hydraulic conductivity values for different samples at different depth are detailed in Table 8.7 and Table 8.8.

In the paleochannel aquifer, the D_{10} value ranges from 0.21 to 0.33 mm, whereas, in alluvial plains, it is 0.14 to 0.18 mm. The value of hydraulic conductivity ranges from

30 to 75.3 m/day for samples falling in the paleochannel, and that between 13.5 to 22.3 m/day for the alluvial plain aquifers.

Hydraulic conductivity data of the paleochannels is not available. The data of hydraulic conductivity of the alluvial plains from Groundwater Department, Uttar Pradesh have been collected for the study area and around. The hydraulic conductivity as determined from pumping test (by UPGWD) varies from 10-48 m/day in the area.

The value of hydraulic conductivity as estimated from the particle size distribution in the present study ranges from 13.5 to 22.3 m/day for the alluvial plain aquifers and from 30 to 75.3 m/day for paleochannel. These values are quite comparable to those determined by the UPGWD.

8.3 Delineation of Paleochannel Aquifer Geometry

The study of aquifer geometry is important as it facilitates identification of areas with favourable aquifer disposition such as aquifer areal extent, thickness, and volume besides, aquifer boundaries and interconnectivity between adjacent aquifers. This information has implications in lateral groundwater movement, water exchange between adjacent aquifers, sea water intrusions, contaminant transport studies, and studies for artificial groundwater recharge (Tait et al., 2004; Srivastava, 2005; Samadder et al., 2007).

Well-log data provide information on lithologic variation with depth, and have been long used for generating sub-surface cross-sections. However, such interpretations have a limitation that the spatial (lateral) control as seen on surface is often not adequate. In this study, remote sensing together with litholog data have been used for interpretating aquifer geometry, as remote sensing data provides valuable information on spatial (lateral) disposition of geological features such as soil, rock types, faults, landforms, drainage, water bodies etc. (Hendrix and Price, 1986; Gupta, 2003, Jaiswal et al., 2003).

As mentioned earlier, paleochannels are quite distinctly seen on the remote sensing images and have hydrogeologic characteristics suitable for artificial groundwater

Table 8.7: D_{10} and hydraulic conductivity (K) values for locations falling in the paleochannel aquifer.

Location Name	Sample No	Depth (m) From	To	D10 (mm)	K (m/day) (Hazen, 1911)
D1	S1	0.0	0.9	0.23	36.5
	S2	0.9	8.5	0.21	30.5
	S3	8.5	12.2	0.22	33.5
	S4	12.2	13.7	0.33	75.3
	S5	13.7	14.6	Pebble	> 100
	S6	14.6	15.8	0.24	39.8
	S7	15.8	16.2	0.25	43.2
	S8	16.2	16.8	0.24	39.8
	S9	16.8	18.3	Pebble	> 100
	S10	18.3	33.5	0.24	39.8
	S11	33.5	39.6	0.21	30.5
D2	S1	0.0	4.6	0.21	30.5
	S2	4.6	9.1	0.23	36.5
	S3	9.1	18.3	0.24	39.8
	S4	18.3	24.4	0.25	43.2
	S5	24.4	25.9	0.22	33.45
	S6	25.9	28.9	Pebble	> 100
	S7	28.9	29.9	Pebble	> 100
	S8	29.9	33.6	0.21	30.5
	S9	33.6	35.7	0.25	43.2
	S10	35.7	38.1	0.21	30.5
	S11	38.1	41.1	0.23	36.5
	S12	41.1	42.2	Pebble	> 100
	S13	42.2	47.5	0.24	39.8
	S14	47.5	48.2	0.21	30.5
	S15	48.2	49.4	Pebble	> 100
	S16	49.4	50.2	Pebble	> 100
	S17	50.2	51.2	0.23	36.5
D3	S1	0.0	9.1	0.25	43.2
	S2	9.1	12.8	0.21	30.5
	S3	12.8	14.0	0.23	36.5
	S4	14.0	15.5	0.22	33.4
	S5	15.5	18.6	0.21	30.5
	S6	18.6	22.5	0.23	36.5
	S7	22.5	24.4	0.21	30.5
	S8	24.4	28.3	Pebble	> 100
	S9	28.3	28.9	0.27	50.38
	S10	28.9	38.1	Pebble	> 100
	S11	38.1	42.7	0.23	36.56
	S12	42.7	47.5	0.21	30.5
	S13	47.5	48.2	0.23	36.5
	S14	48.2	49.4	Pebble	> 100
	S15	49.4	50.3	0.26	46.7

Location Name	Sample No	Depth (m)		D10 (mm)	K (m/day) (Hazen, 1911)
		From	**To**		
D4	S1	0.0	0.6	0.21	30.5
	S2	2.1	4.6	0.21	30.5
	S3	10.8	12.3	0.24	39.8
D5	S1	0.0	0.7	0.24	39.8
	S2	2.3	4.8	0.23	36.5
	S3	6.2	12.4	0.25	43.2
D6	S1	0.0	10.8	0.23	36.56
	S2	10.8	12.3	0.23	39.8
D7	S1	0.0	0.3	0.25	43.2
	S2	4.6	7.7	0.23	35.5
	S3	9.2	12.3	0.21	30.5
D8	S1	0.0	0.6	0.26	46.7
	S2	2.5	4.7	0.25	43.2
	S3	6.0	12.8	0.27	50.38

Table 8.8: D_{10} and hydraulic conductivity (K) values for locations falling in the alluvial plains aquifer.

Location Name	Sample No	Depth (m)		D10 (mm)	K (m/day) (Hazen, 1911)
		From	**To**		
D9	S1	0.0	2.1	0.14	13.5
	S2	2.1	7.6	0.16	17.7
	S3	7.6	12.2	0.16	17.7
D10	S1	0.0	2.1	0.16	17.7
	S2	2.1	10.7	0.16	17.7
	S3	12.2	15.2	0.15	15.6
D11	S1	0.0	3.0	0.14	13.5
	S2	3.0	6.1	0.17	19.9
	S3	6.1	12.2	0.14	13.5
D12	S1	0.0	0.9	0.16	17.7
	S2	0.9	6.1	0.15	15.6
	S3	6.1	7.6	0.16	17.7
	S4	7.6	13.7	0.15	15.6
D13	S1	0.0	2.1	0.14	13.5
	S2	6.1	11.6	0.16	17.7
	S3	12.2	15.2	0.15	15.6
D14	S1	0.0	0.3	0.14	13.5
	S2	2.1	2.7	0.16	17.7
	S3	7.6	9.1	0.16	17.7
	S4	9.1	12.6	0.15	15.6

Table 8.8: (continued from last page)

| Location Name | Sample No | Depth (m) | | D10 (mm) | K (m/day) (Hazen, 1911) |
		From	To		
D15	S1	0.0	3.0	0.14	13.5
	S2	3.0	7.6	0.17	19.97
	S3	7.6	9.1	0.14	13.5
	S4	9.1	10.6	0.18	22.3
	S5	10.6	12.2	0.16	17.7
D16	S1	0.0	3.0	0.14	13.5
	S2	3.0	6.1	0.17	19.97
	S3	6.1	9.1	0.17	19.97
	S4	9.1	12.8	0.17	19.97
	S5	12.8	14.0	0.16	17.7
	S6	14.0	15.2	0.15	15.6
D17	S1	0.0	3.0	0.17	19.97
	S2	3.0	12.80	0.18	22.3
	S3	12.8	15.2	0.18	22.3
	S4	15.2	18.2	0.15	15.6

recharge. Therefore, in this chapter, a systematic approach has been applied to construct paleochannel aquifer geometry and study its interconnectivity with the adjacent aquifers by using well-log and remote sensing data in an interpreted manner.

Methodology for constructing paleochannel aquifer geometry and its interconnectivity with the adjacent aquifers includes — (a) base map preparation, (b) remote sensing image data processing, (c) paleochannel mapping, (c) litholog data analysis, and finally (d) data integration and interpretation (Figure 8.12). The base map preparation, remote sensing image data processing and paleochannel mapping has already been presented. The following sections describe about the litholog data analysis and data integration and interpretation.

8.3.1 Litholog Data Analysis

Litholog data was collected from Tube Well Division of Uttar Pradesh and from field drilling operations in the study area. Figure 8.13 shows the well locations from

which litholog data have been used. It has been observed that the paleochannel aquifer mainly consists of coarse sand occasionally mixed with pebbles, and boulders of varying sizes. On the other hand, the aquifers of the adjacent alluvial plains are mainly composed of medium to fine grained sand along with clay and kankar beds. A surficial clay layer (thickness 0.8-2 m), which is supposed to be responsible for high surface runoff, is present in the alluvial plains, whereas, it is generally absent over the paleochannels.

8.3.2 Data Integration and Interpretation

Construction of subsurface lithological cross-section, construction of aquifer geometry, and final interpretation has been made by aggregating and synthesizing all the information - such as the base map, the CIR composite image, the paleochannel map, well location map, and the DEM.

The most of the bore logs collected from the Tuble Well Division of Uttar Pradesh are pertained to non-paleochannel area. They also have a large variation in strata penetrated, level of details, and lithological description. The existing lithologs are compared and standardised with respect to the observed field data and analyzed using Rockworks software.

For analysis of litholog data in Rockworks, the following inputs are required: location of the well-logs, log names, ground elevation of the corresponding wells, sub-surface lithologies and their respective depth from the ground level at which they occur.

From the topographic map, a DEM has been generated; the wells were located on the DEM and the heights corresponding to the wells are determined by overlying the locations on the DEM.

All these informations, such as well location, name and corresponding surface height, UTM coordinates, and the sorted lithological information of the individual well including depth data of lithologies were entered into Rockworks for analysis and interpretation. The litholog data were sorted out and different lithological units were classified as aquifer and confining layers. After this, a well location map was displayed in Rockworks and single litholog for each well and numerous cross-sections between wells were constructed to aid interpretation.

8.3.3 Interpretation and Construction of Aquifer Geometry

The various data sets and maps, including the base map, the CIR composite image, and paleochannel map were converted into UTM coordinate system and imported into Rockworks. Interpretation has been done by aggregating and synthesizing all the information. Figure 8.13 shows the CIR composite in the background with well locations for which the litholog information has been used. Also shown are the lineament and paleochannels interpreted from remote sensing data.

Various cross-sections along strike of the paleochannel, across the paleochannel and within the paleochannel are studied and are critically analyzed for interpreting geometry and interconnectivity of the paleochannel aquifer with the adjacent alluvial aquifer. A few typical interpreted geological sections are given below (Figure 8.14 to Figure 8.17, horizontal and vertical scale is given along side of each profile):

8.4 Natural Groundwater Recharge Estimation by Tritium Tracer Technique

Estimation of natural groundwater recharge is very important for artificial groundwater recharge study and various groundwater applications such as groundwater budgeting and planning groundwater usage. Surface infiltration systems designed to provide artificial recharge of groundwater require permeable soils (sandy loam, sands, gravel) that must have relatively high recharge rate so that the water can be transmitted adequately. A proper understanding of soil moisture movement in the unsaturated zone is of importance in understanding and estimating the groundwater recharge. There are two components of recharge to groundwater: (i) vertical component, which includes precipitation and irrigation inputs, and (ii) lateral component, through the subsurface horizontal flow due to natural hydraulic gradient. In most of the cases, the major source of recharge to groundwater is due to precipitation. There has been an increasing emphasis on the use of isotopic and tracer techniques for soil moisture movement analysis and estimating groundwater recharge in the unsaturated zone. The advantage is that the tritiated water molecule, HTO, does not behave differently from the other water molecules in the ground water cycle. The health hazard in handling tritium is also negligible because of its emission of soft beta particles having maximum energies of only

18 KeV. Several workers (Zimmerman et al., 1967a, 1967b; Munnich 1968a, 1968b; Datta et al., 1973; Sukhija et al., 1996) have applied the tritium tagging methods for soil moisture movement analysis in unsaturated zones of different geological and climatological conditions.

Although, the study area is a part of vast Indo-Gangetic Plains which are broadly categorized as an alluvial region, there exists variation in landforms with varying soil and hydrogeologic characteristics which are likely to control the recharge rate. Besides the main channel of the Ganga River, there are two major landforms — paleochannels and alluvial plains in the area (Figure 8.18). Hence, in this section, groundwater recharge rate due to precipitation is estimated using tritium tagging technique in two major different landforms, viz. the paleochannels and the alluvial plains over the study area. The landform map generated from remote sensing (IRS-LISS-II multispectral sensor) data is used as a base map for selecting sites for tritium injection. Adequate field data (grain size distribution of soil samples, water table fluctuation etc.) has been used as ground truth for verifying and supporting the interpretations. Field hydrogeological characteristics of the paleochannel and the adjacent alluvial plains have already been **discussed in Chapter 5.** The following section describes methodology of the work (Figure 8.19)-site selection for tritium injection, field and laboratory experiment, and finally results.

8.4.1 Site Selection

Keeping in view the aim of the present study to estimate natural groundwater recharge in the areas of two different landforms, sites for tritium injection have been selected using landform and paleochannel map generated from remote sensing data. Fourteen experimental sites — eight within paleochannel and six on the alluvial plains, have been selected .

8.4.2 Injection of Tritium at the Selected Sites

Tritium injection experiment is performed during the pre-monsoon period (June 2006). At each selected site, five injections of 2 ml tritium of 40μ Ci/cc specific activity were made within a circle of 0.1 m radius (one at the center and the other four along the

circumference on the extremities of two mutually perpendicular diameters) at a depth of about 70 cm below ground level (Figure 8.20). A precise identification was given to each injection site. The holes were back-filled with the same soil after injecting tritium in order to reduce the direct loss of injected tracer due to evaporation and to avoid the direct entry of water.

8.4.3 Soil Sampling

The soil samples were collected just before injection (in June, 2006) and after about four months of injection (in October, 2006) at each 10 cm vertical soil column. Soil samples were collected layer by layer with the help of a hand auger of 2 inch diameter from ground surface to about 250 cm depth (Figure 8.21). The soil sample from each layer was carefully weighed and about 200 gm of the sample was collected in properly sealed polyethylene bottles so that there was no exchange of the moisture with the atmosphere.

8.4.4 Soil Moisture Content Estimation

The moisture content of the soil samples on wet weight basis was estimated by gravimetric method. Weight of each sample was determined by weighing the samples using electronic balance. After that, a small amount of soil sample (approximately 100 gm) was kept in oven at 108^0 C for 24 hours to dry. Calculating the weight difference between wet and dry sample, the percentage of moisture content present in the soil sample was estimated. Bulk density for each soil sample was determined by dividing the wet weight of the sample by the volume of each sample, which was equivalent to the volume of hand auger of known diameter (2 inches) for 10 cm depth of soil column. Volumetric moisture content for each soil sample was estimated by multiplying the moisture content and bulk density of the soil.

8.4.5 Tritium Activity Measurement with LSC

Tritium activity was measured on liquid scintillation counter (LSC) (Model 'System 1409', Wallac Oy, Finland) at Nuclear Hydrology Laboratory of National Institute of Hydrology, Roorkee, India, by standard methodology. The values of volumetric moisture contents and net tritium count rate of different sites are tabulated in Annexure I.

8.4.6 Determination of Recharge to Groundwater

Munnich (1968a, 1968b) and Zimmerman et al. (1967a, 1967b) initiated the use of isotope technique to monitor the vertical movement of water. They assumed that the moisture flows in discrete layers in such a way that if any fresh water is added to the top surface of the soil, the infiltrated layer of the water pushes the older layer downward in the soil system and so on till the last layer of moisture reaches the saturated zone. This concept of water flow in unsaturated zone is known as the piston flow model. Thus, if a radio-isotope (say tritium) is tagged below the active root zone (below 70 cm) and not affected by solar heating, the tagged tritium will be mixed with the soil moisture available at that depth and will act as an impermeable sheet. Therefore, water added to the top of the soil surface will infiltrate into the ground by pushing down the older water. Thus the shift in the tritium peak can be observed after some time.

The net tritium count rates for various sites were plotted as a histogram against the individual depth intervals, which shows position of the original and shifted peaks of the injected tritium. The movement of injected tritium and soil moisture at various test sites are shown in Figure 8.22. The shift of the peak from original depth of injection of 70 cm was calculated. Percent recharge to the groundwater during time interval between injection of tritium and subsequent sampling (pre-monsoon to post-monsoon 2006) has been calculated using the following equation (Zimmerman et al. 1967a, 1967b):

$$R = Q_v \, d \, (100/P)$$

Where, R: the percentage of recharge to ground water

Q_v: the effective average volumetric moisture content in tritium peak shift region.

d : the shift of tritium peak in cm, and

p: precipitation and irrigation inputs in cm at the injection site. These two components are taken for the interval between injection and sampling. However, all the stations considered in this study are on non-irrigated patches.

Table 8.9: The percentage recharge to groundwater at various experimental sites due to monsoonal rain.

Location	Tritium Peak Shift (d) in cm	Average effective volumetric moisture content (Q_v) in peak shift region	Precipitation (cm) between injection time to sampling time	Recharge to groundwater (%)
(a) Paleochannel				
T1	165.0	0.077	67.3	18.9
T 2	175.0	0.079	67.3	20.4
T3	155.0	0. 099	67.3	23.0
T4	153.0	0.122	65.3	28.7
T5	95.3	0.189	67.3	26.8
T6	75.4	0.143	67.3	16.0
T7	75.2	0.151	67.3	17.0
T8	57.0	0.201	67.3	17.0
(b) Alluvial Plains				
T9	32.0	0.176	67.3	8.4
T10	30.8	0.184	67.3	8.4
T11	24.0	0.176	67.3	6.3
T12	30.8	0.196	67.3	8.9
T13	31.9	0.198	67.3	9.4
T14	39.9	0.187	67.3	11.0

The precipitation data was collected from the Groundwater Department, Uttar Pradesh, India. The rainfall distribution map was generated from Thiessen polygon

method through GIS and subsequently the total monsoon (from the date of injection to the date of sampling) rainfall was calculated for each experimental site. The movement of injected tritium and soil moisture at a typical test site is shown in Figure 8.22. The computed recharge rates at various experimental sites, as determined from field cum laboratory data of tritium peak shift, average volumetric moisture content in peak shift region and precipitation (in the time interval of injection and sampling) are given in Table 8.9.

Analysis of particle size distribution of soil samples collected form different sites was carried out by sieve analysis. The test results of the analysis for various sites are given in Annexure-II. Figure 8.23 represents the relationship between average sand content (%) and recharge rate for both the landform types. It is observed that the plot between percentage of average sand content and recharge rates shows a linear relationship In the paleochannel areas, the percentage of sand content is high (80.5-93.7%) and recharge rates are also high. On the other hand, in the alluvial plains, the sand content is lower (41.9-51.3 %) and recharge rates are also much lower.

By comparing recharge rates with different landforms and their hydrogeologic characteristics, it can be inferred that: (a) paleochannel area has relatively coarse grained material with sandy loam soil type and having high recharge rate of 17.0 to 28.7%, and (b) the upper layers of the alluvial plains have medium to fine grained sediments with silty loam soil type showing relatively low recharge rate (6.3 to 11.0 %).

8.5 Groundwater Flow

Groundwater flow map has been generated to establish the groundwater flow direction. For this purpose, groundwater levels have been monitored in wells at 37 locations (12 on the paleochannel aquifers and 25 on the adjacent alluvium plains) over 2 years (2006-2007) for both pre- and post-monsoon period (Table 8.10). The precise locations (x, y, z co-ordinates) have been determined through differential GPS.

Average depth to water level below ground surface for each observation wells has been determined for both pre- and post-monsoon period. The reduced groundwater level for each well has been obtained by subtracting the value of depth to water level below ground surface to the ground height of the observation points. The longitudes/latitudes

Table 8.10: Groundwater level data used in the present study.

Aquifers	Location ID	Ground height from msl (m).	Depth of WT (m) from GL			
			Pre-monsoon		Post-monsoon	
			2006	2007	2006	2007
Paleochannel	W1	255.35	5.90	6.30	5.70	5.80
	W2	253.67	4.53	4.53	3.86	3.88
	W3	254.45	7.54	7.56	7.10	7.10
	W4	250.16	4.70	4.76	4.56	4.57
	W5	250.03	3.92	4.00	3.91	3.95
	W6	248.37	5.79	5.81	4.49	4.51
	W7	241.12	6.60	6.64	6.48	6.52
	W8*	246.97	13.10	12.85	12.93	12.69
	W9*	246.96	14.82	14.84	14.46	14.48
	W10	242.71	8.23	8.23	7.56	7.60
	W11	237.85	8.90	9.00	8.74	8.78
	W12	239.08	6.04	6.12	5.60	5.66
Alluvium plains	W13	255.39	5.05	5.09	3.07	3.09
	W14	255.92	6.36	6.42	5.45	5.49
	W15	254.29	3.31	3.33	1.55	1.61
	W16	254.86	5.20	5.30	3.60	3.68
	W21	251.97	6.96	6.98	4.00	4.01
	W22	244.16	8.35	8.37	8.19	8.21
	W23	245.23	7.40	7.40	7.16	7.18
	W24	245.30	7.95	7.99	7.67	7.67
	W25	239.15	7.81	7.83	7.66	7.68
	W26	239.23	6.01	6.05	5.80	5.80
	W27	242.30	7.62	7.64	5.30	5.36
	W28	241.02	9.61	9.65	8.61	8.61
	W29	236.94	9.99	9.99	9.94	9.96
	W30	241.71	11.59	11.61	10.65	10.68
	W31	239.50	5.78	5.80	3.28	3.30
	W32	240.74	7.86	7.84	6.10	6.12
	W33	256.50	6.49	6.51	6.00	6.00
	W34*	253.63	3.42	3.44	2.79	2.81
	W35*	251.46	3.99	3.97	3.51	3.53
	W36*	249.00	4.00	4.00	4.00	4.00
	W37	250.70	10.76	11.78	11.46	11.48

* Locations near the distributary

and ground height of each observation wells were obtained from differential GPS. The X, Y co-ordinates (i.e. longitude/latitude) of each well and their corresponding reduced groundwater level are stored as point attribute file in GIS. The file is then exported from GIS in the text (.txt) format, which is then used to generate a grid data using the 'Data operation' from the Grid menu in Surfer software by using Krigging interpolation method. The resultant grid thus produced has been used to generate reduced water level contour map and flow vector map using 'Contour Map' and 'Vector Map' operation from the main menu of the Surfer software. The vector spacing has been taken to be 20 m in both the X and Y direction. Integrated interpretation has been made by combining information of paleochannel map, reduced water level contour map and flow direction map. The longitudes/latitudes and ground level (GL) height from mean sea level (MSL), and corresponding water table (WT) depth from GL of each observation wells are given in Table 8.10. The well location map, for which the groundwater flow direction maps have been generated, is shown in Figure 8.24. The reduced groundwater level contour maps along with flow direction and paleochannel map for both pre- and post monsoon period are shown in Figure 8.24b and Figure 8.25. It has been observed that groundwater flows away from the paleochannel for both pre- and post-monsoon period. The typical contour pattern (convex downwards) in the paleochannel aquifer is interpreted to be due to its higher vertical hydraulic conductivity and porosity. This further indicates that recharging of groundwater through paleochannels would lead to gradually recharging the alluvial plains.

The values of specific yield were determined during the present study using the following equation given by Gupta and Sharma (1984):

$$S = \frac{Q}{\partial h * A}$$

Where, S = specific yield

A = Area of thiessain polygon (m^2).

Q = Quantity of estimated recharge in the polygon area (m^3).

= A × Average fractional recharge × Rainfall in meter

∂h = Average water level fluctuation for the polygon area during the period

of the tritium experiment (m).

For point location, Equiation-1 can be written as

$$S = \frac{\text{Average fractional recharge} \times \text{Rainfall in meter}}{\text{Average water level fluctuation during the period of the tritium experiment}}$$

Based on the above equation, specific yield values for few sites are estimated as given in Table below.

Table 8.11: Specific yield values for selected sites

Location	Fractional Recharge	Sand %	Water Level Fluctuation (m)	Specific Yield (%)
(a) Paleochannel				
T1	0.19	80.50	0.45	28.3
T2	0.20	83.80	0.52	25.8
T3	0.23	88.20	0.67	23.0
T4	0.29	93.70	1.21	16.8
(b) Alluval plains				
T9	0.084	49.80	0.41	13.7
T11	0.063	41.90	0.40	10.6
T12	0.089	51.30	0.42	14.2

It has been observed that the paleochannel aquifer shows higher specific yields (16.8 to 28.3%) than that of adjacent shallow aquifer (specific yield is less than 14.2%). The average value of specific yield have also been reported by Shakeel (1997) over the study area, which ranges from 13 to 26%. So, the specific yield values obtained by the combine use of tritium tracer along with relevant field data shows a good correlation with field data.

9. Conclusion/Recommendation

In the present work, a systematic study has been taken up to explore the possibility of replenishing groundwater artificially in the study area, lying in the western part of the Indo-Gangetic Plains. The main objectives of the research work are: (a) application of

Remote Sensing — GIS techniques to map spatial distribution of porous and permeable stretches, which happen to be parts of paleochannels of the Ganga river, and (b) evaluation of hydrogeological characteristics of the paleochannel-aquifers and also the adjacent alluvial plains.

The IRS-1B LISS-II multispectral data have been co-registered with the base map, and corrected for atmospheric path radiance and striping, and enhanced for improving interpretability. The IRS-1B-LISS-II sensor data has been used as the primary data source to implement the supervised classification for generating landuse/landcover (LULC) map. Six LULC classes - agricultural land, paleochannel, dry streams, water body, built-up area, and marshy land, have been chosen and a LULC map has been generated with an overall accuracy of 87.9% using Maximum Likelihood Classifier (MLC). Finally, integrating information from colour infra-red composites and LULC map, a paleochannel map has been generated. The existence of paleochannels has also been cross-checked from litholog data and field observations.

In the study area, three major paleochannels characterized by serpentine and meandering pattern, have been deciphered. The paleochannels are located to the west of the present day course of the river Ganga. Most of the paleochannels are very wide (4-6 km) suggesting their formation by a large river. It can be inferred that the Ganga river has gradually shifted from the west to the east. Field observations have revealed that the soils in the paleochannels are generally coarse sand. Rather sparse vegetation and low surface moisture over the paleochannel areas are indicative of highly permeable, porous, coarse grained materials possessing high infiltration rate. This is amply indicated by the spectral characteristics such as, very light tone in NIR band, and yellowish-white colour in CIR composites.

The litholog data have been analysed to determine aquifer depth and lithological details. It has been observed that the paleochannel aquifer mainly consists of coarse sand occasionally mixed with pebbles, and boulders of varying sizes. On the other hand, the aquifers of adjacent alluvial plains are mainly composed of medium to fine grained sand along with clay and kankar beds.

Construction of subsurface lithological cross-section, construction of paleochannel aquifer geometry and its inter-connectivity with the adjacent alluvial plains

aquifer has been done by aggregating and synthesizing all the information, such as the lithological information, the base map, the CIR composite image, paleochannel map, well location map, and the DEM. The first aquifer ($\approx$ 25-30 m thick) in the alluvial plains is unconfined and consists of fine to medium sand with several lenses of clay and kankar. The second aquifer is confined in nature and mainly consists of fine to medium grained sand along with some lenses of kankar. The paleochannel aquifer is unconfined and is mainly composed of coarse sandy material along with boulder and pebbles beds. This paleochannel aquifer extends upto a depth of about 65 m and is well inter-connected with the adjacent alluvial aquifers.

A series of 17 observation wells systematically sited on the paleochannel and its either flanks have been drilled and sampling has been carried out for collecting lithological information at different depths. Grain size analysis has been conducted for 82 samples. Based on grain-size analyses and the use of the Hazen (1911) equation, the bulk hydraulic conductivity for selected core samples at different depths has been estimated. It is found that the value of hydraulic conductivity ranges from 30 to 75.3 m/day for samples falling in the paleochannel, and that between 13.5 to 22.3 m/day for the alluvial plain aquifers.

The natural groundwater recharge rate due to precipitation has been estimated using tritium tagging technique. Comparison of recharge rates and hydrogeologic characteristics in different landforms indicates that: (a) paleochannel area have coarse grained soil (sandy loam) and high recharge rate of 18.9 to 28.7%, and (b) the alluvial plains have medium to fine grained soil (silty loam) and relatively lower recharge rate (6.3 to 8.9 %).

Groundwater levels have been monitored at 37 locations (12 on the paleochannel aquifers and 25 on the adjacent alluvial plains aquifer) over 2 years (2006-2007) for both pre- and post-monsoon period. The precise locations (x, y, z co-ordinates) have been determined through differential GPS. Interpretation have been made by combining information of paleochannel map, reduced water level contour map and flow direction map. It has been observed that groundwater flows away from the paleochannel in both pre- and post-monsoon period, which is related to the high hydraulic conductivity and porosity of the paleochannel aquifer. This further indicates that recharging of

groundwater through paleochannels would lead to gradually recharging of the aquifers in the alluvial plains.

10. How do the conclusion/recommendations compare with current Thinking?

Till now, generally throughout the world, the paleochannels have been considered as exploration sites for the supply of ground water, as paleochannels are porous and permeable and they may have subsurface link to river courses. However, in this study it is considered that in the foothill zones of mountains and adjoining plains, the upper reaches of paleochannels where ground water may occur at deeper levels, can be considered as potential sites for artificial ground water recharge. In this way, this can be considered as a new type of application having potential for resource augmentation.

11 Field tests conducted - Described above in section 8

12 Softwares generated if any - Nil

13 Possibilities of any patents/copyrights. If so then action taken in this regard - Nil

14 Suggestions for further work

The above data and results show that:

a) There occur wide (4-6 km) and extensive (60-80 km long) stretches of palaeochannels of the Ganga river in the area, which are highly porous and permeable. The paleochannel aquifers comprise of dominantly coarse sand with occasional pebbles and possess very high hydraulic conductivity (30–75.3 m/day).

b) The paleochannel aquifers are found to extend up-to a depth of >60 m below the surface and appear to be laterally interconnected with other adjacent aquifers in the alluvial plains.

c) The recharge rate is much higher (upto 28.7%) in the areas of paleochannels than in the areas of general alluvial plains (upto 8.9%). Further, specific yield is found

to be 16.8–28.3% in the paleochannel aquifers, as compared to <14.2% in the alluvial shallow aquifers.

d) The groundwater contour map exhibits typical convex downwards pattern in the paleochannel aquifer areas for both pre- and post-monsoon data sets; this indicates higher hydraulic conductivity and porosity in the paleochannel region. This further shows that if groundwater is recharged through paleochannels, it will gradually recharge the alluvial plains also.

In view of the above, it is inferred that the upper parts of the paleochannels can be possibly used as sites of artificial ground water recharge, to augment and replenish the depleting ground water resources.

It is recommended that future investigation particularly involving local and regional ground water modeling be carried out to assess the potential and also implications of these sites for artificial ground water recharge.

References

Anderson, J. M., Hardy, E. E., Roach, J. T. and Witmert, R. E., (1976) A Land Use Classification System for Use with Remote Sensing Data, *U. S. Geological Survey Professional Paper*, No. 964, Washington DC: Government Printing Office.

Brown, R., B., (1990) Soil Texture, Fact sheet SL-29, Soil and Water Science Department, Florida Cooperative Extension Service, Institute of Food and Agricultural Sciences, University of Florida.

Bouwer, H., (2002) Artificial Recharge of Groundwater: Hydrogeology and Engineering, *Hydrogeology Journal*, 10, 121-142.

Carver, R. E., (1971) Procedure in Sedimentary Petrology, *Wily-Interscience*, Division of John Wiley & Sons.

Chavez, P. S. Jr., (1988) An Improved Dark Object Subtraction Technique for Atmospheric Correction of Multispectral Data, *Remote Sensing of Environment*, 24, 459-479.

Csaplovics, E., (1998) High Resolution Space Imagery for Regional Environmental Monitoring – Status Quo and Future Trends, *International Archives of Photogrammetry & Remote Sensing*, 32(7), 211-216.

Datta, P. S., Goel, P. S. and Rama Sangal, S. P., (1973) Groundwater Recharge in Western Uttar Pradesh, *Proceedings of Indian Academy of Sciences*, LXXV, 1-12.

Fetter, C. W., (1994) Applied Hydrogeology: Englewood Cliffs, New Jersey, Prentice-Hall, 691p.

Foody, G. M., (2002) Status of Land Cover Classification Accuracy Assessment, *Remote Sensing of Environment,* 80, 185-201.

Gupta, R. P., (2003) Remote Sensing Geology, 2nd Edition, *Springer-Verlag*, Berlin-Heidelberg, Germany, 655p.

Hazen, A., (1911) Discussion—Dams on Sand Foundations: In Transactions, *American Society of Civil Engineers*, 73, 199p.

Hendrix, W. G. and Price, J. E., (1986) Application of Geographic Information Systems for Assessment of Site Index and Forest Constraints, *Proceedings of the GIS workshop*, ASPR, Falls Church Vernia, 368-377.

Jaiswal, R. K., Mukherjee, S., Krishnamuthy, J. and Saxena, R., (2003) Role of Remote Sensing and Geographic Information System Techniques for Generating of Ground Water Prospect Zones Towards Rural Development - An Approach, *International Journal of Remote Sensing*, 24**,** 993-1008.

Jensen, J. R. (1996) Introductory Digital Image Processing-A Remote Sensing Perspective, 2nd Edition, *Prentice-Hall*, New Jersey, US, 379p.

Kumar, S., Parkash, B., Manchanda, M. L. and Singhvi, A. K., (1996) Holocene Landform and Soil Evolution of the Western Gangetic Plains: Implications of Neotectonics and Climate, *Z. Geomorph. N.F*., Suppl.-Bd 103, 283-312.

Mather, P. M., (1999) Computer Processing of Remotely-Sensed Images: An Introduction, 2nd Edition, *Willey*, Chichester, UK, 306p.

Munnich, K. O., (1968a) Moisture Movement Measured by Isotope Tagging, *In: Guide Book on Nuclear Techniques in Hydrology*, International Atomic Energy Agency, Vienna, 112-117.

Munnich, K. O., (1968b) Use of Nuclear Techniques for the Determination of Groundwater Recharge Rates, *In: Guide Book on Nuclear Techniques in Hydrology*, International Atomic Energy Agency, Vienna, 191-197.

National Bureau of Soil Survey and Land Use Planning, (1999) Soil Map of Uttar Pradesh, Sheet No.1, Scale 1: 500,000.

National Institute of Hydrology (NIH), (1986) Hydrogeological Investigation in Sabarmati and Mahi Basins and Coastal Saurahtra using Radioisotopes and Chemical Tracers - A Report, NIH, Roorkee, India.

National Institute of Hydrology (NIH), (2000) Study of Soil Moisture Movement and Recharge to Groundwater due to Monsoon Rains and Irrigation using Tritium Tagging Technique in Saharanpur District, NIH, Roorkee, India, Report No. CS/AR-23/1999-2000.

Samadder, R. K., Kumar, S. and Gupta, R. P., (2007) Conjunctive Use of Well-log and Remote Sensing Data for Interpreting Shallow Aquifer Geometry in Ganga Plains, *Journal of the Geological Society of India*, 69, 925-932.

Srivastava, A., (2005) Aquifer Geometry, Basement-topography and Groundwater Quality around Ken Graben, India, *Journal of Spatial Hydrology*, 2(2), 1-7.

Sukhija, B. S., Nagabhushanam, P. and Reddy, D. V., (1996) Groundwater Recharge in Semi-arid Regions of India: An Overview of Results Obtained Using Tracers, *Hydrogeology Journal*, 4, 51-71.

Tait, N. G., Davison, R. M., Whittaker, J. J., Leharne, S. A. and Lerner, D. N., (2004) Borehole Optimization System (BOS) - A GIS Based Risk Analysis Tool for Optimizing the Use of Urban Groundwater, *Environmental Modeling and Software*,19, 1111-1124.

Zimmerman, U., Ehhalt, D. and Munnich, K. O., (1967a) Soil Water Movement and Evapotranspiration: Changes in Isotopic Components of Soil Water, In: *Isotopes in Hydrology*, Proceedings Symposium, Vienna, 567-585.

Zimmerman, U., Munnich, K. O. and Roether, W., (1967b) Downward Movement of Soil Moisture Traced by Means of Hydrogen Isotopes, In: *Glenn ES (ed) Isotope techniques in the hydrologic cycle*: American Geophysical Union, Geophysical Monograph, 11, 28-36.

ANNEXURE-I

Volumetric soil moisture content and net tritium count rate at location T-1.

Depth (cm)	Volumetric moisture content (%)		Net tritium counts per minute
	Pre-Monsoon	**Post-Monsoon**	
0-10	0.0064	0.0681	22.0
10-20	0.0209	0.0476	31.4
20-30	0.0718	0.0896	11.8
30-40	0.0494	0.1275	14.2
40-50	0.0577	0.1060	11.4
50-60	0.0537	0.1094	28.2
60-70	0.0536	0.1117	60.6
70-80	0.0558	0.0939	35.4
80-90	0.0509	0.0934	27.2
90-100	0.0546	0.1095	30.0
100-110	0.0545	0.1063	22.4
110-120	0.0584	0.1065	47.2
120-130	0.0641	0.1190	47.0
130-140	0.0615	0.1180	52.4
140-150	0.0558	0.1238	89.2
150-160	0.0743	0.1227	199.0
160-170	0.0614	0.1118	276.4
170-180	0.0655	0.1106	479.0
180-190	0.0662	0.1065	644.4
190-200	0.0585	0.1079	850.0
200-210	0.0596	0.0968	1021.2
210-220	0.0540	0.1070	1136.8
220-230	0.0551	0.1114	1190.0
230-240	0.0538	0.1008	1216.6
240-250	0.0530	0.0911	1089.4

Volumetric soil moisture content and net tritium count rate at location T-2.

Depth (cm)	Volumetric moisture content (%)		Net tritium counts per minute
	Pre-Monsoon	Post-Monsoon	
0-10	0.0062	0.0476	9.0
10-20	0.0377	0.1252	20.6
20-30	0.0654	0.1322	6.0
30-40	0.0920	0.1405	18.8
40-50	0.1051	0.1558	8.0
50-60	0.0898	0.1435	53.4
60-70	0.0876	0.1273	25.4
70-80	0.0716	0.1332	31.2
80-90	0.0791	0.1361	34.6
90-100	0.0730	0.1472	25.4
100-110	0.0465	0.1048	13.0
110-120	0.0722	0.1260	20.4
120-130	0.0645	0.1022	21.8
130-140	0.0713	0.0920	36.0
140-150	0.0698	0.0807	72.8
150-160	0.0776	0.0805	125.8
160-170	0.0834	0.0797	237.6
170-180	0.0780	0.0978	340.8
180-190	0.0790	0.0847	528.6
190-200	0.0723	0.0904	691.8
200-210	0.0752	0.1001	968.8
210-220	0.0741	0.0866	1299.2
220-230	0.0777	0.0819	1318.0
230-240	0.0759	0.1077	1439.0
240-250	0.0684	0.0889	1650.8

Volumetric soil moisture content and net tritium count rate at location T-3.

Depth (cm)	Volumetric moisture content (%)		Net tritium counts per minute
	Pre-Monsoon	**Post-Monsoon**	
0-10	0.0334	0.0659	40.2
10-20	0.0640	0.1159	20.0
20-30	0.0975	0.1354	22.3
30-40	0.1202	0.1721	22.6
40-50	0.1335	0.1577	18.0
50-60	0.1219	0.1463	12.6
60-70	0.1234	0.1285	41.2
70-80	0.1238	0.1309	30.8
80-90	0.1444	0.1881	32.0
90-100	0.1512	0.1605	49.0
100-110	0.1786	0.1898	34.6
110-120	0.1464	0.1567	41.4
120-130	0.1528	0.1818	70.6
130-140	0.1175	0.1570	75.0
140-150	0.1458	0.1497	118.6
150-160	0.1200	0.1469	235.4
160-170	0.1263	0.1469	400.4
170-180	0.0983	0.1517	635.0
180-190	0.0881	0.1427	900.2
190-200	0.0824	0.1556	1318.5
200-210	0.0798	0.1289	1349.2
210-220	0.0708	0.12087	1408.0
220-230	0.0689	0.1309	1456.2
230-240	0.0818	0.1298	1260.2
240-250	0.0753	0.1056	1000.4

Volumetric soil moisture content and net tritium count rate at location T-4.

Depth (cm)	Volumetric moisture content (%)		Net tritium counts per minute
	Pre-Monsoon	Post-Monsoon	
0-10	0.0703	0.0424	42.2
10-20	0.0613	0.1150	14.0
20-30	0.1017	0.1268	23.8
30-40	0.1109	0.1798	22.6
40-50	0.1284	0.1705	19.0
50-60	0.1082	0.1583	11.6
60-70	0.0972	0.1168	42.2
70-80	0.0879	0.1072	35.8
80-90	0.0488	0.1251	34.8
90-100	0.0968	0.1141	48.0
100-110	0.0887	0.1161	33.6
110-120	0.0956	0.1298	40.4
120-130	0.0795	0.1192	71.6
130-140	0.0888	0.1235	73.0
140-150	0.0894	0.1105	120.6
150-160	0.0663	0.1309	230.4
160-170	0.0626	0.1256	398.4
170-180	0.0705	0.1393	634.0
180-190	0.0959	0.1499	898.2
190-200	0.0724	0.1341	1311.6
200-210	0.0610	0.1480	1337.2
210-220	0.0890	0.1241	1403.2
220-230	0.1051	0.1399	1453.2
230-240	0.0871	0.1479	1280.2
240-250	0.1045	0.1539	42.2

Volumetric soil moisture content and net tritium count rate at location T-5.

Depth (cm)	Volumetric moisture content (%)		Net tritium counts per minute
	Pre-Monsoon	**Post-Monsoon**	
0-10	0.0436	0.1426	18.2
10-20	0.0762	0.1553	22.9
20-30	0.1055	0.1394	19.6
30-40	0.1262	0.1056	15.2
40-50	0.1004	0.0798	20.4
50-60	0.0565	0.0699	17.6
60-70	0.0398	0.0668	24.9
70-80	0.0268	0.0730	25.6
80-90	0.0247	0.0711	26.3
90-100	0.0263	0.0756	29.2
100-110	0.0187	0.0847	23.5
110-120	0.0279	0.0873	18.7
120-130	0.0343	0.2570	15.0
130-140	0.0540	0.3072	35.9
140-150	0.1884	0.5313	55.4
150-160	0.1124	0.1946	130.7
160-170	0.0696	0.2125	219.9
170-180	0.0870	0.2485	183.2
180-190	0.0889	0.2733	78.9
190-200	0.1168	0.3466	56.1
200-210	0.1207	0.3933	41.7
210-220	0.1068	0.3382	34.3
220-230	0.0535	0.3807	21.3
230-240	0.0576	0.4423	17.1
240-250	0.0594	0.5293	16.8

Volumetric soil moisture content and net tritium count rate at location T-6.

Depth (cm)	Volumetric moisture content (%)		Net tritium counts per minute
	Pre-Monsoon	**Post-Monsoon**	
0-10	0.0584	0.0429	29.3
10-20	0.0980	0.1198	33.7
20-30	0.1055	0.1520	28.2
30-40	0.0314	0.1352	77.4
40-50	0.0976	0.1102	107.1
50-60	0.0973	0.1247	141.4
60-70	0.0642	0.1251	138.8
70-80	0.0326	0.1585	159.1
80-90	0.0379	0.1567	185.0
90-100	0.0324	0.1661	235.7
100-110	0.0382	0.1395	484.6
110-120	0.0256	0.0636	921.6
120-130	0.0240	0.1539	1783.8
130-140	0.0178	0.1740	2361.7
140-150	0.0299	0.1301	2455.7
150-160	0.0388	0.1136	2951.6
160-170	0.0305	0.1027	1812.2
170-180	0.0324	0.1061	1303.2
180-190	0.0385	0.2060	260.7
190-200	0.0786	0.370	1 80.0
200-210	0.2122	0.4114	42.0
210-220	0.1850	0.4461	59.7
220-230	0.1068	0.2946	43.7
230-240	0.2344	0.4716	50.0
240-250	0.2038	0.4441	24.3

Volumetric soil moisture content and net tritium count rate at location T-7.

Depth (cm)	Volumetric moisture content (%)		Net tritium counts per minute
	Pre-Monsoon	**Post-Monsoon**	
0-10	0.1987	0.2187	16.8
10-20	0.3730	0.2452	30.1
20-30	0.2381	0.3202	27.2
30-40	0.3062	0.3853	28.3
40-50	0.2683	0.3791	33.7
50-60	0.4060	0.2066	35.5
60-70	0.2714	0.1894	29.2
70-80	0.2282	0.1370	29.3
80-90	0.2283	0.1533	13.7
90-100	0.1545	0.2036	36.5
100-110	0.1593	0.1618	38.6
110-120	01964	0.1103	44.9
120-130	0.1298	0.1773	111.3
130-140	0.1433	0.1167	206.9
140-150	0.1928	0.1532	314.4
150-160	0.2014	0.1242	105.1
160-170	0.1191	0.1048	119.4
170-180	0.1230	0.1364	120.3
180-190	0.1086	0.1739	91.4
190-200	0.1285	0.2161	45.8
200-210	0.1066	0.1337	38.6
210-220	0.1064	0.1534	30.6
220-230	0.1786	0.1993	31.3
230-240	29.208	0.3954	53.3
240-250	36.596	0.4805	14.7

Volumetric soil moisture content and net tritium count rate at location T-8.

Depth (cm)	Volumetric moisture content (%)		Net tritium counts per minute
	Pre-Monsoon	**Post-Monsoon**	
0-10	0.0614	0.0236	35.6
10-20	0.1275	0.0870	32.4
20-30	0.7846	0.0547	28.2
30-40	0.1012	0.0795	27.2
40-50	0.1795	0.1530	20.0
50-60	0.2269	0.2717	45.9
60-70	0.1588	0.2968	41.7
70-80	0.1198	0.1786	53.1
80-90	0.1193	0.1850	106.6
90-100	0.1091	0.3734	257.7
100-110	0.0935	0.2590	494.8
110-120	0.0383	0.1190	621.7
120-130	0.0269	0.0930	744.0
130-140	0.0293	0.0656	680.7
140-150	0.0498	0.1277	531.0
150-160	0.2049	0.4986	259.6
160-170	0.1865	0.5835	116.4
170-180	0.1748	0.6307	56.6
180-190	0.1898	0.6326	34.6
190-200	0.2001	0.4554	30.3
200-210	0.1775	0.3707	49.0
210-220	0.1348	0.2476	29.0
220-230	0.0569	0.3283	64.5
230-240		0.3293	42.0

Volumetric soil moisture content and net tritium count rate at location T-9.

Depth (cm)	Volumetric moisture content (%)		Net tritium counts per minute
	Pre-Monsoon	**Post-Monsoon**	
0-10	0.0639	0.0713	22.4
10-20	0.1334	0.1664	0.0
20-30	0.1821	0.2039	9.4
30-40	0.2715	0.1990	0.0
40-50	0.1446	0.2051	19.6
50-60	0.2216	0.1499	67.2
60-70	0.2249	0.1670	197.4
70-80	0.1624	0.1445	470.4
80-90	0.2119	0.3223	712.4
90-100	0.2145	0.1609	872.8
100-110	0.2024	0.1501	948.2
110-120	0.1555	0.1349	939.4
120-130	0.1436	0.1743	819
130-140	0.1745	0.1892	438.6
140-150	0.1422	0.1958	347.4
150-160	0.1396	0.1214	650.8
160-170	0.1417	0.1962	221.4
170-180	0.1399	0.1620	140.0
180-190	0.1114	0.2218	88.4
190-200	0.1230	0.2078	66.8
200-210	0.0832	0.2315	27.2
210-220	0.0765	0.1819	46.4
220-230	0.0614	0.1667	17.2
230-240	0.0598	0.1133	74.6
240-250	0.0750	0.1580	38.0

Volumetric soil moisture content and net tritium count rate at location T-10.

Depth (cm)	Volumetric moisture content (%)		Net tritium counts per minute
	Pre-Monsoon	**Post-Monsoon**	
0-10	0.1106	0.0924	35.4
10-20	0.1741	0.1645	34.4
20-30	0.2129	0.1489	32.3
30-40	0.2339	0.1407	40.6
40-50	0.2541	0.1866	45.8
50-60	0.2811	0.2054	69.8
60-70	0.3072	0.2360	202.5
70-80	0.1582	0.2316	577.4
80-90	0.1086	0.2201	1375.9
90-100	0.1137	0.1375	1702.9
100-110	0.0939	0.1489	1476.6
110-120	0.0710	0.1267	1074.9
120-130	0.1577	0.1848	624.6
130-140	0.1056	0.0951	295.0
140-150	0.1917	0.1130	157.9
150-160	0.1493	0.2050	94.6
160-170	0.2218	0.2194	69.7
170-180	0.2143	0.1817	77.0
180-190	0.1571	0.2110	50.0
190-200	0.1597	0.2034	49.6
200-210	0.2606	0.1665	49.7
210-220	0.1082	0.1702	81.2
220-230	0.1017	0.1739	69.8
230-240	0.1133	0.1654	92.5
240-250	0.1734	0.1408	61.4

Volumetric soil moisture content and net tritium count rate at location T-11.

Depth (cm)	Volumetric moisture content (%)		Net tritium counts per minute
	Pre-Monsoon	**Post-Monsoon**	
0-10	0.0253	0.085118	104.8
10-20	0.0739	0.101476	126.8
20-30	0.0829	0.130095	104.8
30-40	0.1033	0.140576	166.0
40-50	0.1011	0.158760	183.0
50-60	0.1068	0.209530	352.4
60-70	0.1247	0.157272	878.4
70-80	0.1452	0.185593	1798.2
80-90	0.1753	0.192702	3279.2
90-100	0.1514	0.201712	4298.6
100-110	0.1343	0.159581	3235.6
110-120	0.1227	0.189425	1869.2
120-130	0.1561	0.153764	797.4
130-140	0.1139	0.237928	376.6
140-150	0.1431	0.205099	537.4
150-160	0.1491	0.103899	197.4

Volumetric soil moisture content and net tritium count rate at location T-12.

Depth (cm)	Volumetric moisture content (%)		Net tritium counts per minute
	Pre-Monsoon	**Post-Monsoon**	
0-10	0.0924	0.1106	35.4
10-20	0.1645	0.1741	34.4
20-30	0.1489	0.2129	32.3
30-40	0.1407	0.2339	40.6
40-50	0.1866	0.2541	45.8
50-60	0.2054	0.2811	69.8
60-70	0.2360	0.3072	202.5
70-80	0.2316	0.1582	577.4
80-90	0.2201	0.1086	1375.9
90-100	0.1375	0.1137	1702.9
100-110	0.1489	0.0939	1476.6
110-120	0.1267	0.0710	1074.9
120-130	0.1848	0.1577	624.6
130-140	0.0951	0.1056	295.0
140-150	0.1130	0.1917	157.9
150-160	0.2050	0.1493	94.6
160-170	0.2194	0.2218	69.7
170-180	0.1817	0.2143	77.0
180-190	0.2110	0.1571	50.0
190-200	0.2034	0.1597	49.6
200-210	0.1665	0.2606	49.7
210-220	0.1720	0.1082	81.2
220-230	0.1739	0.1017	69.8
230-240	0.1654	0.1133	92.5
240-250	0.1408	0.1734	61.4

ANNEXURE-II

Particle size distribution for site T1.

Sl. No.	Depth (m)	Sand % (2 mm-0.075 mm)	(Silt+Clay) % (<0.075 mm)
1.	0-50	71.1	28.9
2.	50-100	85.4	14.6
3.	100-150	82.6	17.4
4	150-200	85.8	14.2
5.	200-250	77.4	22.6
Average		**80.5**	**19.5**

Particle size distribution for site T2.

Sl. No.	Depth (m)	Sand % (2 mm-0.075 mm)	(Silt+Clay) % (<0.075 mm)
1.	0-50	74.9	25.1
2.	50-100	93.7	6.3
3.	100-150	83.8	16.2
4	150-200	87.7	12.3
5.	200-250	78.9	21.1
Average		**83.8**	**16.2**

Particle size distribution for site T3.

Sl. No.	Depth (m)	Sand % (2 mm-0.075 mm)	(Silt+Clay) % (<0.075 mm)
1.	0-50	84.8	15.2
2.	50-100	87.9	12.1
3.	100-150	88.6	11.4
4	150-200	89.3	10.7
5.	200-250	90.5	9.5
Average		**88.2**	**11.8**

Particle size distribution for site T4.

Sl. No.	Depth (m)	Sand % (2 mm-0.075 mm)	(Silt+Clay) % (<0.075 mm)
1.	0-50	89.8	10.2
2.	50-100	93.5	6.5
3.	100-150	94.6	5.4
4	150-200	95.2	4.8
5.	200-250	95.5	4.5
Average		**93.7**	**6.3**

Particle size distribution for site T5.

Sl. No.	Depth (m)	Sand % (2 mm-0.075 mm)	(Silt+Clay) % (<0.075 mm)
1.	0-50	88.06	11.93
2.	50-100	91.02	8.97
3.	100-150	83.87	16.12
4	150-200	85.74	14.25
5.	200-250	88.97	11.02
Average		**87.53**	**12.46**

Particle size distribution for site T6.

Sl. No.	Depth (m)	Sand % (2 mm-0.075 mm)	(Silt+Clay) % (<0.075 mm)
1.	0-50	89.06	10.93
2.	50-100	74.40	25.60
3.	100-150	82.33	17.67
4	150-200	87.90	12.10
5.	200-250	82.98	17.02
Average		**83.33**	**16.66**

Particle size distribution for site T7.

Sl. No.	Depth (m)	Sand % (2 mm- 0.075 mm)	(Silt+Clay) % (<0.075 mm)
1.	0-50	76.49	23.50
2.	50-100	78.77	21.22
3.	100-150	86.29	13.71
4	150-200	92.46	7.54
5.	200-250	90.20	9.80
Average		**84.84**	**15.15**

Particle size distribution for site T8.

Sl. No.	Depth (m)	Sand % (2 mm- 0.075 mm)	(Silt+Clay) % (<0.075 mm)
1.	0-50	93.4	6.60
2.	50-100	85.18	14.82
3.	100-150	86.38	13.62
4	150-200	73.96	26.04
5.	200-250	78.54	21.46
Average		**83.49**	**16.50**

Particle size distribution for site T9.

Sl. No.	Depth (m)	Sand % (2 mm- 0.075 mm)	(Silt+Clay) % (<0.075 mm)
1.	0-50	26.5	73.5
2.	50-100	54.8	45.2
3.	100-150	52.2	47.8
4	150-200	56.9	43.1
5.	200-250	58.8	41.2
Average		**49.8**	**50.2**

Particle size distribution for site T10.

Sl. No.	Depth (m)	Sand % (2 mm-0.075 mm)	(Silt+Clay) % (<0.075 mm)
1.	0-50	83.05	16.94
2.	50-100	79.87	20.12
3.	100-150	80.08	19.92
4	150-200	86.59	13.61
5.	200-250	64.48	35.51
Average		**78.81**	**21.22**

Particle size distribution for site T11.

Sl. No.	Depth (m)	Sand % (2 mm-0.075 mm)	(Silt+Clay) % (<0.075 mm)
1.	0-50	28.4	71.6
2.	50-100	41.7	58.3
3.	100-150	48.6	51.4
4	150-200	46.8	53.2
5.	200-250	44.1	55.9
Average		**41.9**	**58.1**

Particle size distribution for site T12.

Sl. No.	Depth (m)	Sand % (2 mm-0.075 mm)	(Silt+Clay) % (<0.075 mm)
1.	0-50	31.3	68.7
2.	50-100	56.8	43.2
3.	100-150	55.2	44.8
4	150-200	55.8	44.2
5.	200-250	57.1	42.9
Average		**51.3**	**48.7**

Figures

Figure 7.1: Drilling conducted on the paleochannel near Berla village. (a) Machine operated 'Bukki System' and (b) Different parts of 'Bukki System'.
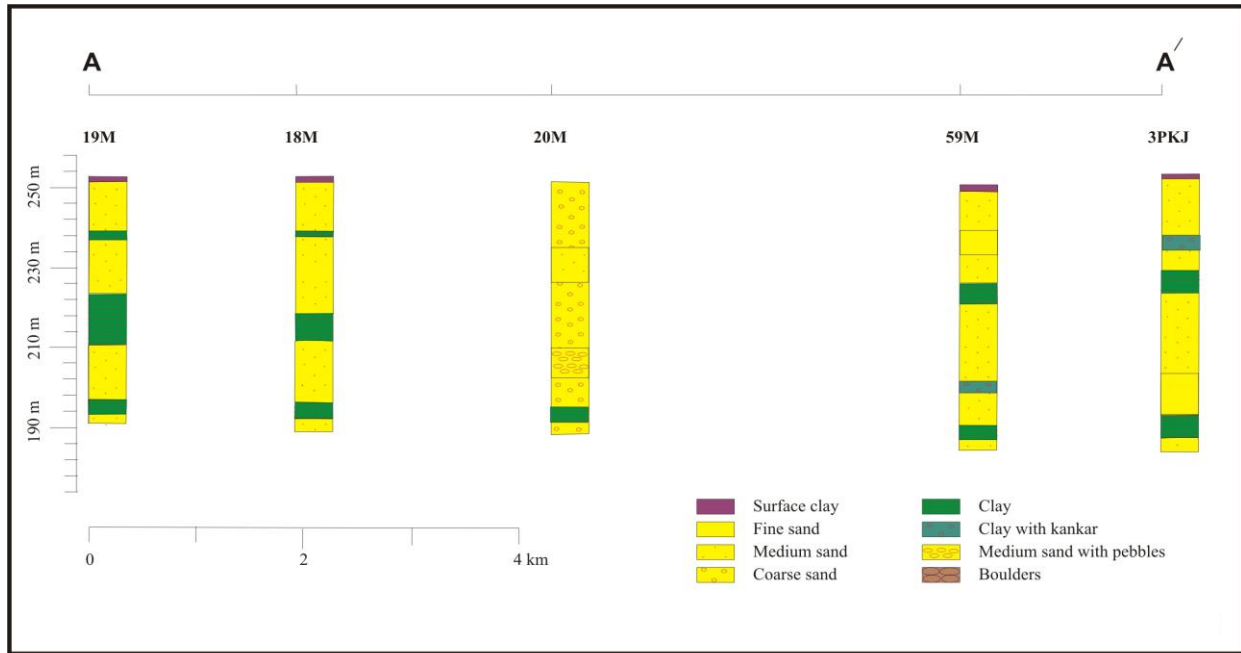
Figure 7.2: Lithologic description of wells 19M, 18M, 20M, 59M and 3PKJ.
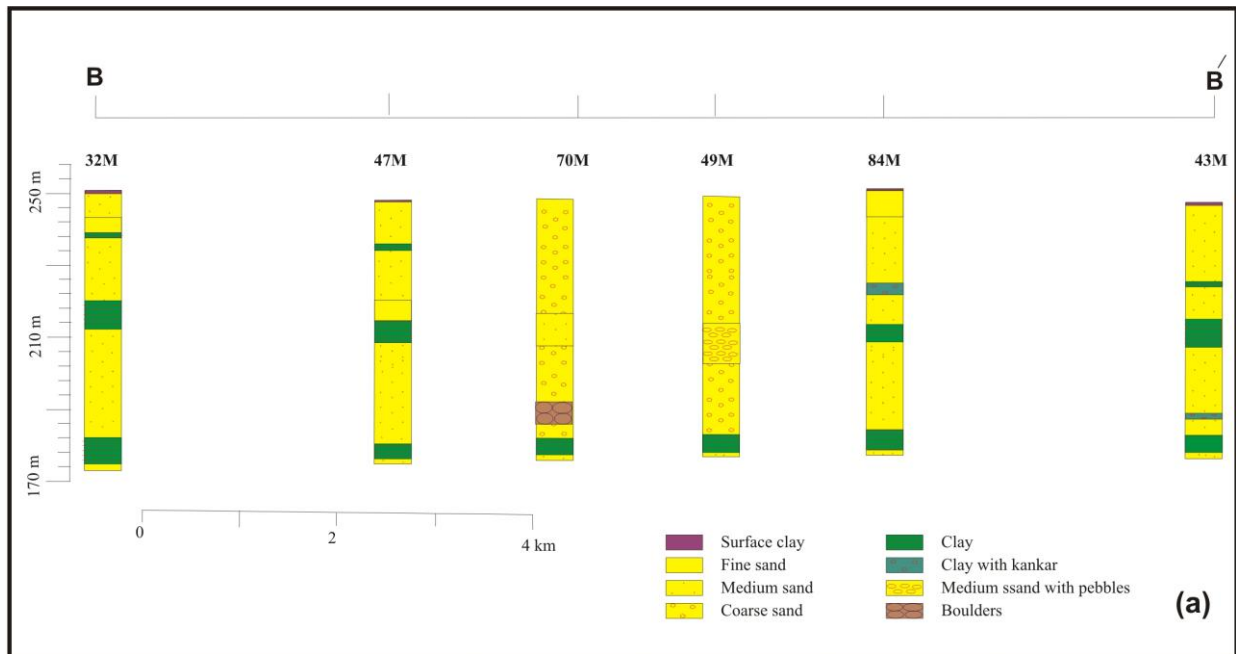
Figure 7.3: Lithologic description of wells 32M, 47M, 70M, 49M, 84M and 43M.
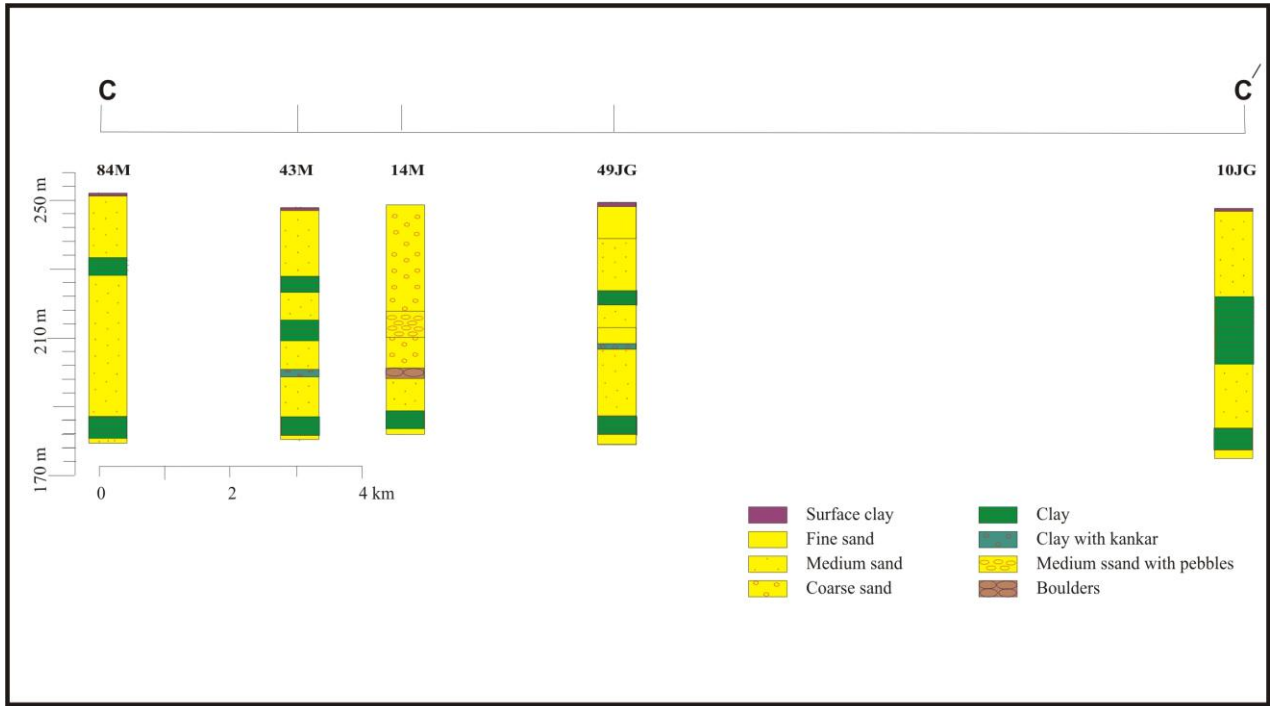
Figure 7.4: Lithologic description of wells 84M, 43M, 14M, 69M and 10JG.
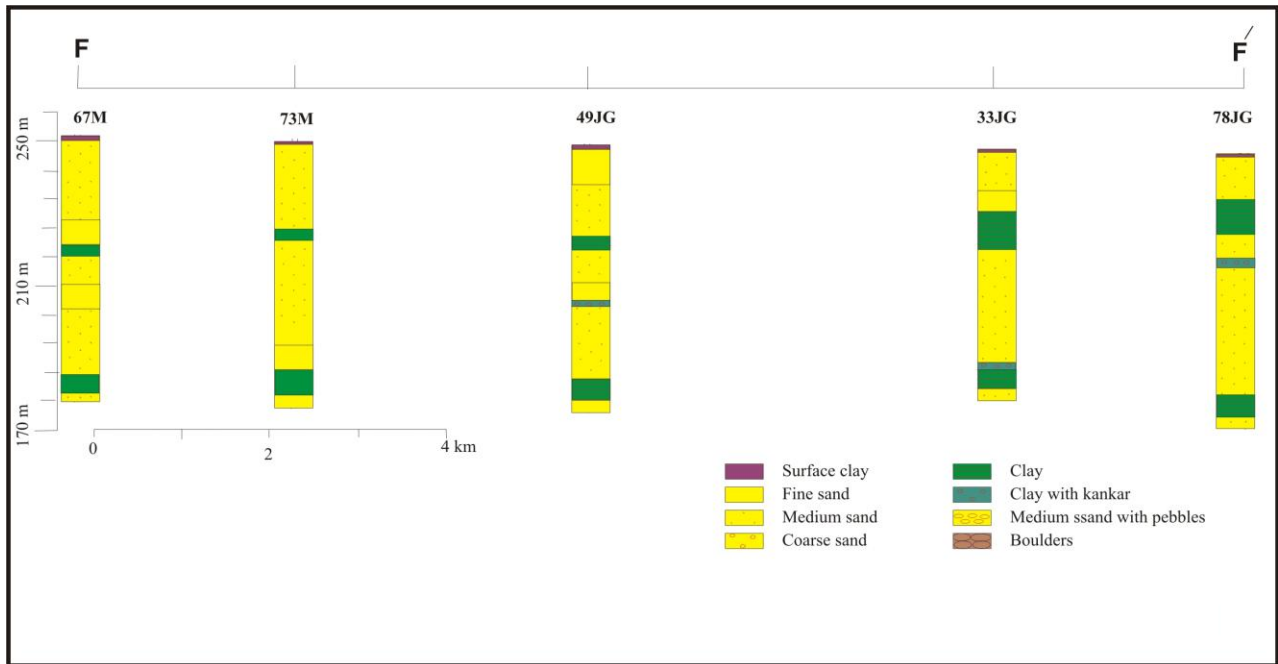
Figure 7.5: Lithologic description of wells 67M, 73M, 49JG, 33JG and 78JG.
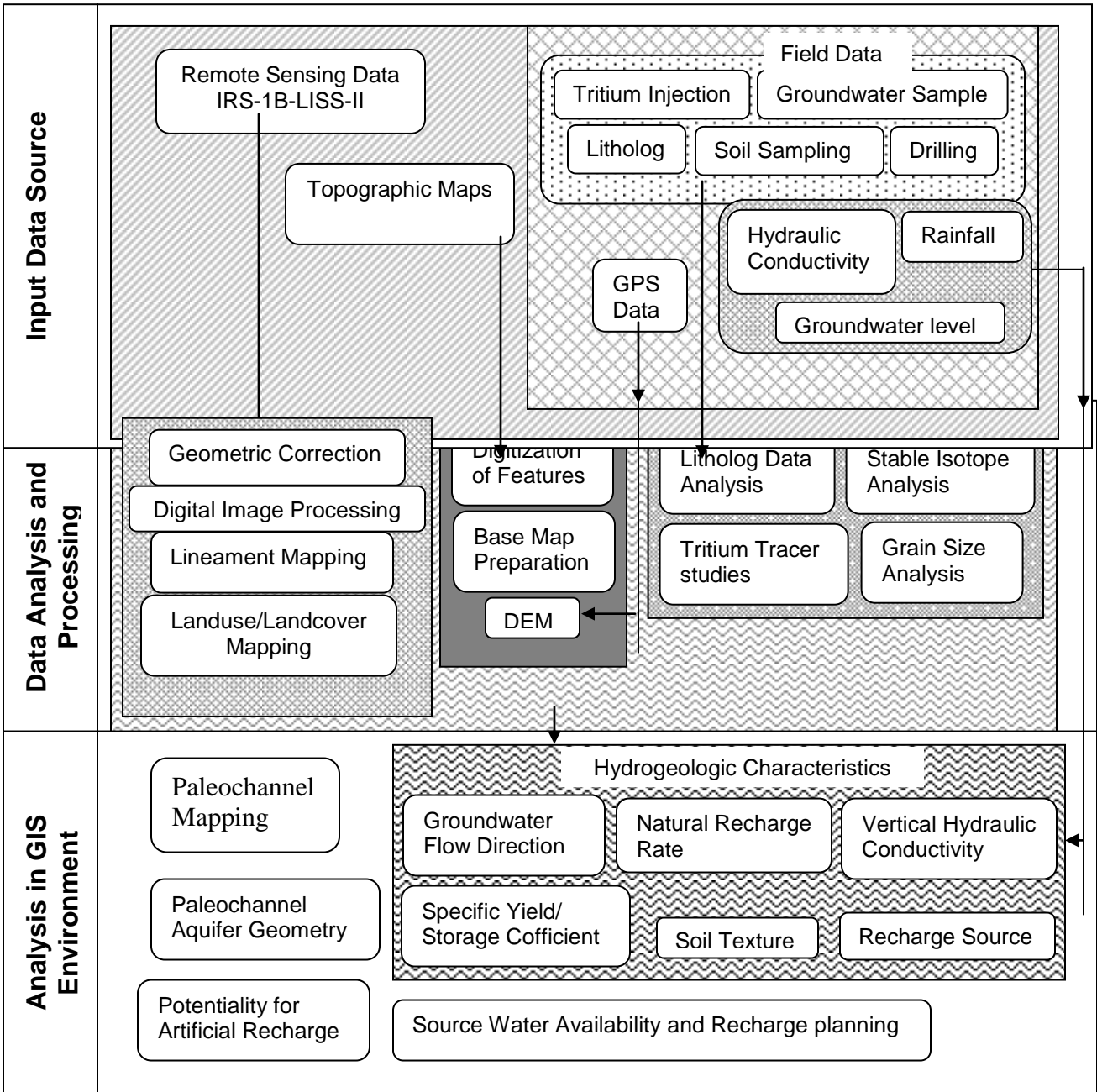
Figure 8.1: Flow diagram showing the broad methodology adopted in this study.
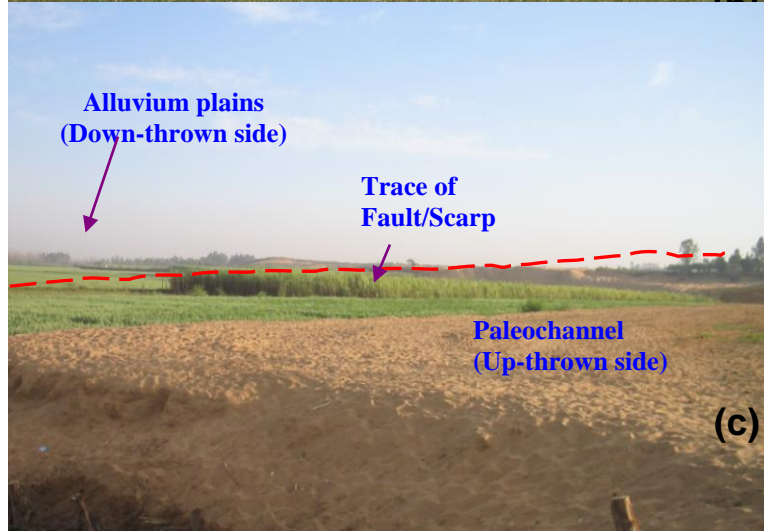
Figure 8.2: Field photographs. (a) Paleochannel near Barla village (note the scant vegetation and agricultural activity and presence of coarse sand); (b) Agricultural field in the alluvial plains and (c) Trace of Fault/Scarp near Harinagar village.
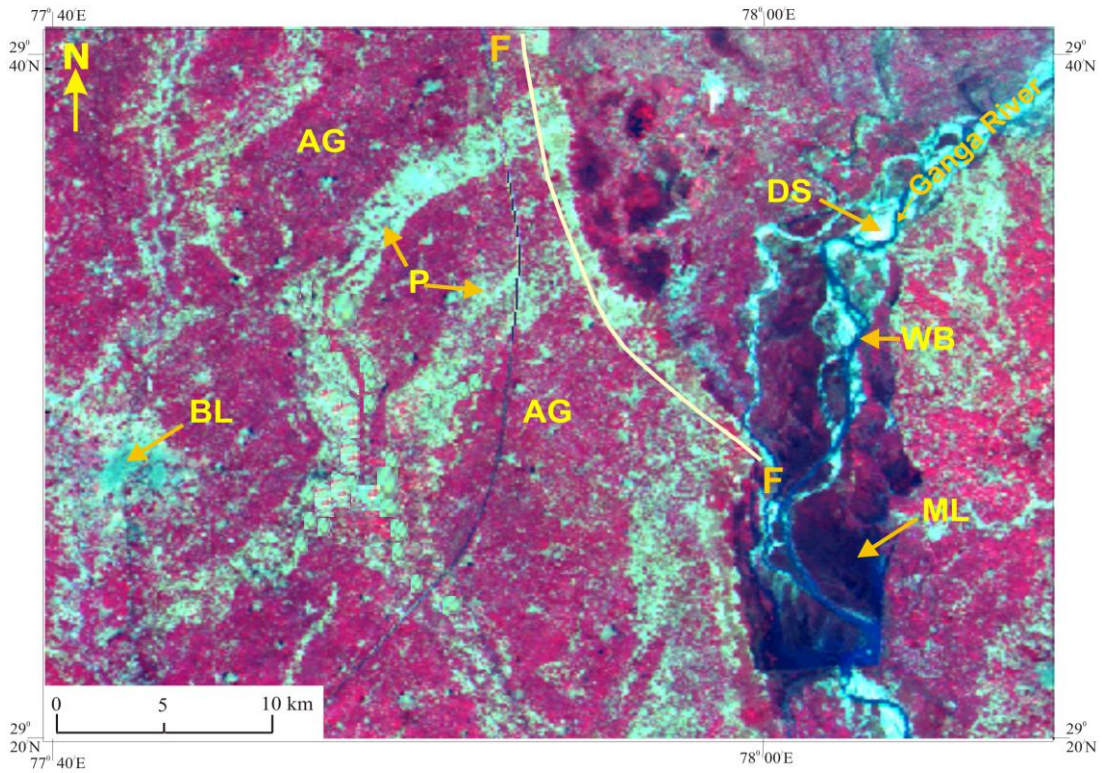
Figure 8.3: Colour infra-red composite of LISS-II image (NIR band coded in red colour; Red band codded in green colour and Green band coded in blue colour) showing various LULC classes (AG-Agricultural lands; P-Paleochannel; BL- Built-up areas; ML-Marshy lands; WB-Water body DS-Dry stream/flood plains and F-F: Fault scarp).
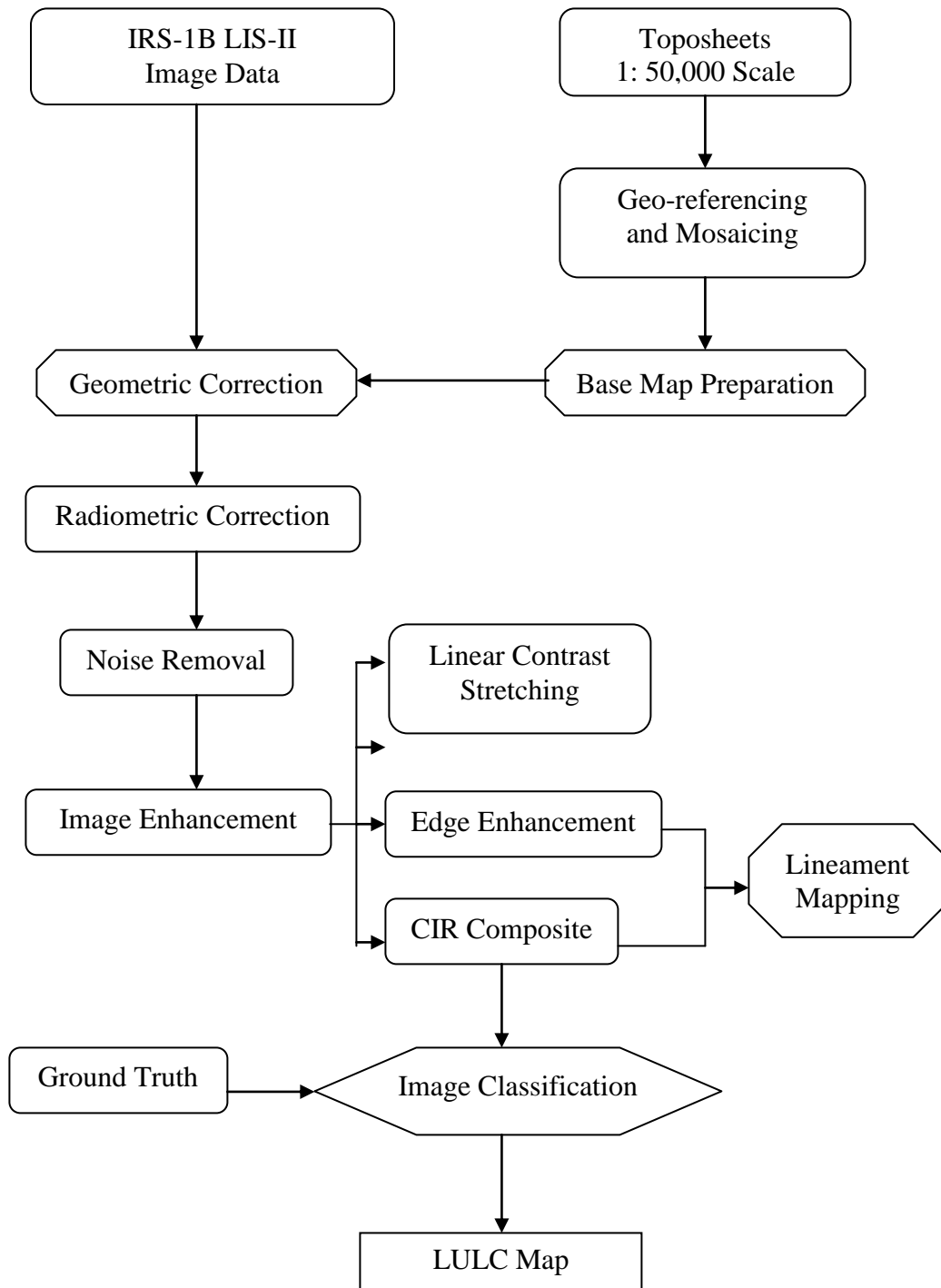
Figure 8.4: Flow diagram showing image processing techniques adopted in the study.
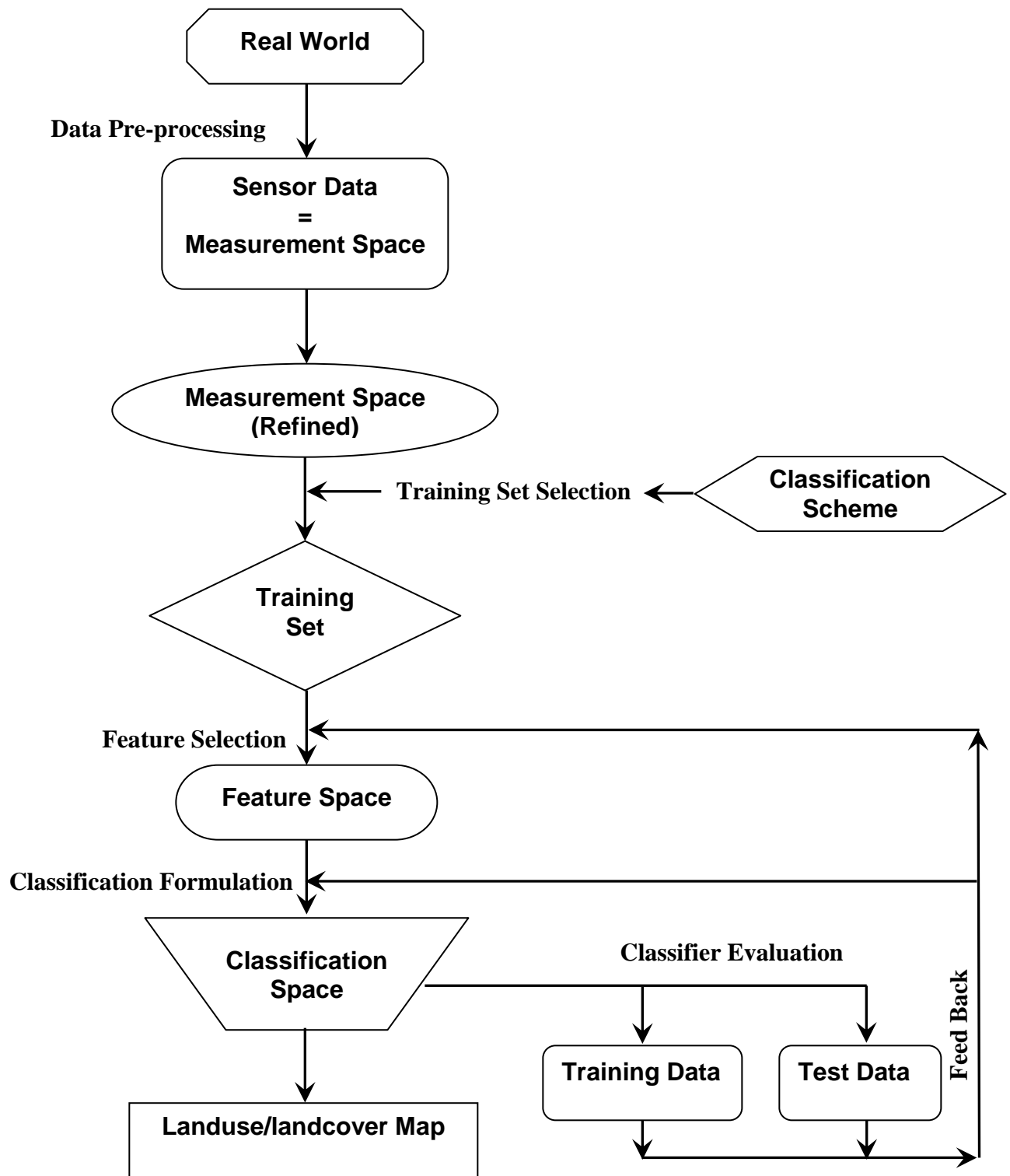
Figure 8.5: Supervised classification approach adopted in this study.
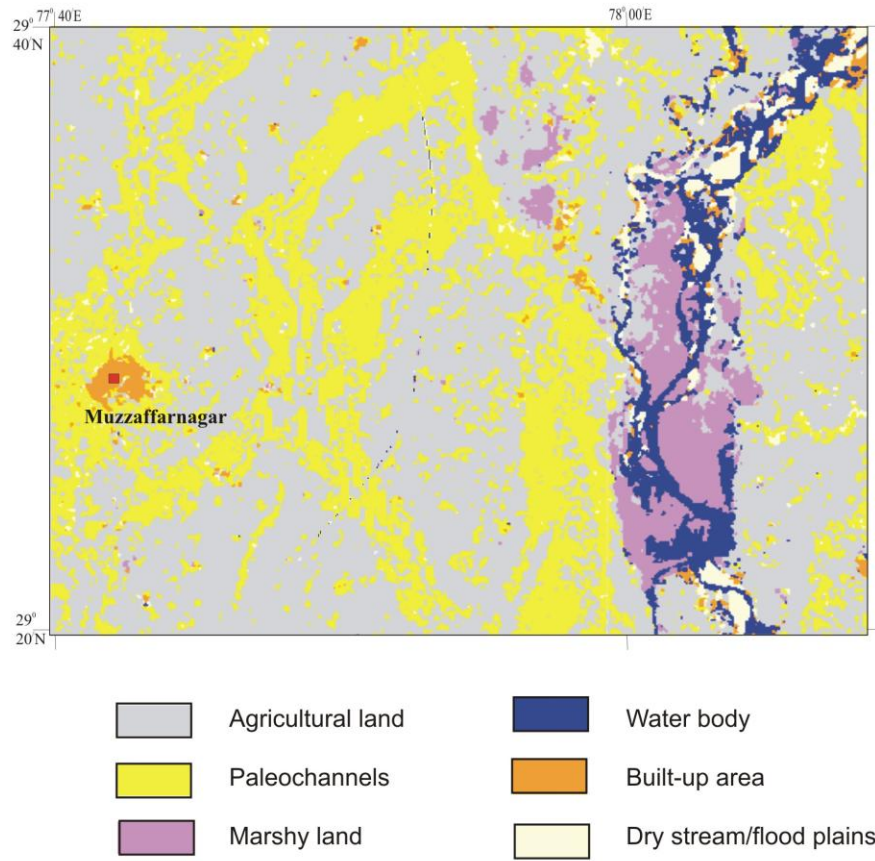
Figure 8.6: Landcover map possessing accuracy of 87.9% generated from band combination 4, 1, 2,3 (i.e. NIR, Red, Green and Blue bands of LISS-II image). A post-classification filtering has been applied.
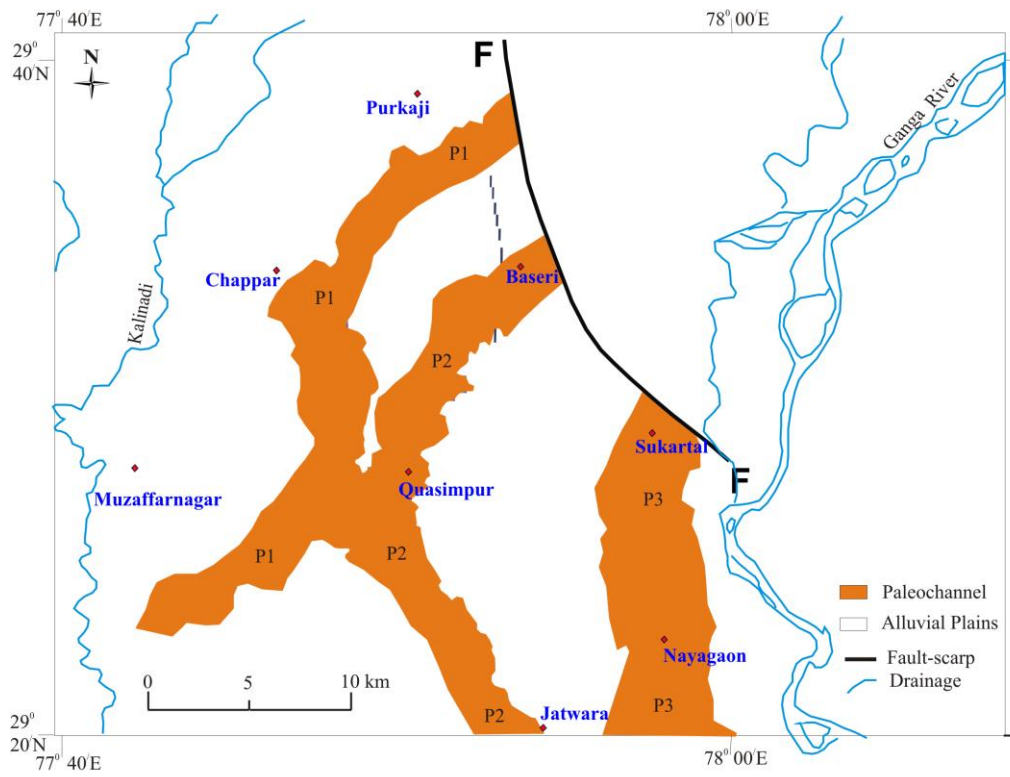
Figure 8.7: Major paleochannels of the study area.
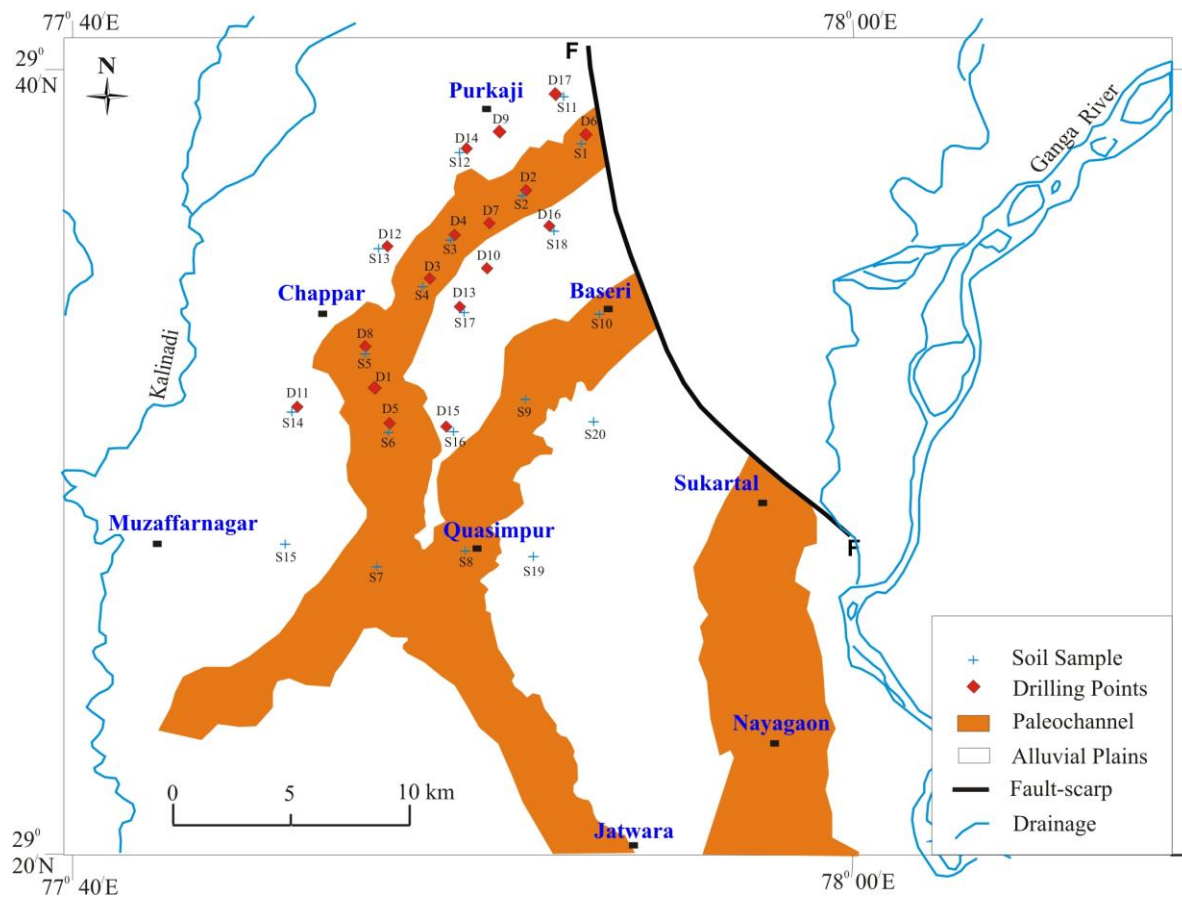
Figure 8.8: Location map of soil samples and drilling sites.
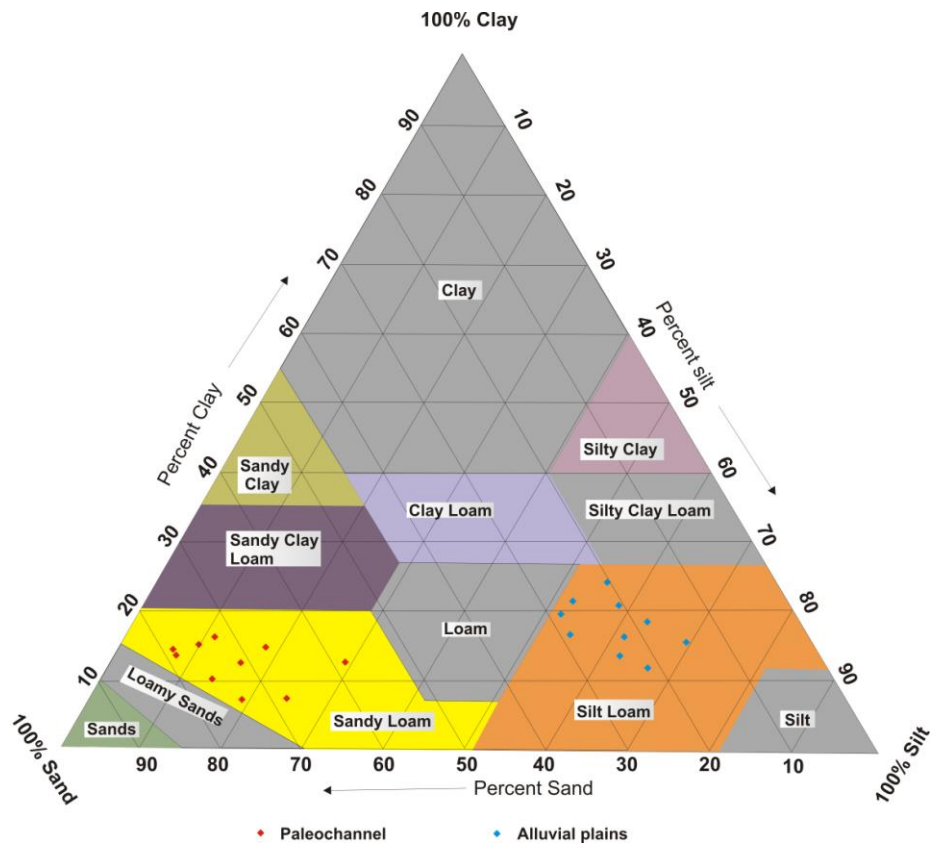
Figure 8.9: Soil samples plotted on USDA soil textural triangle.
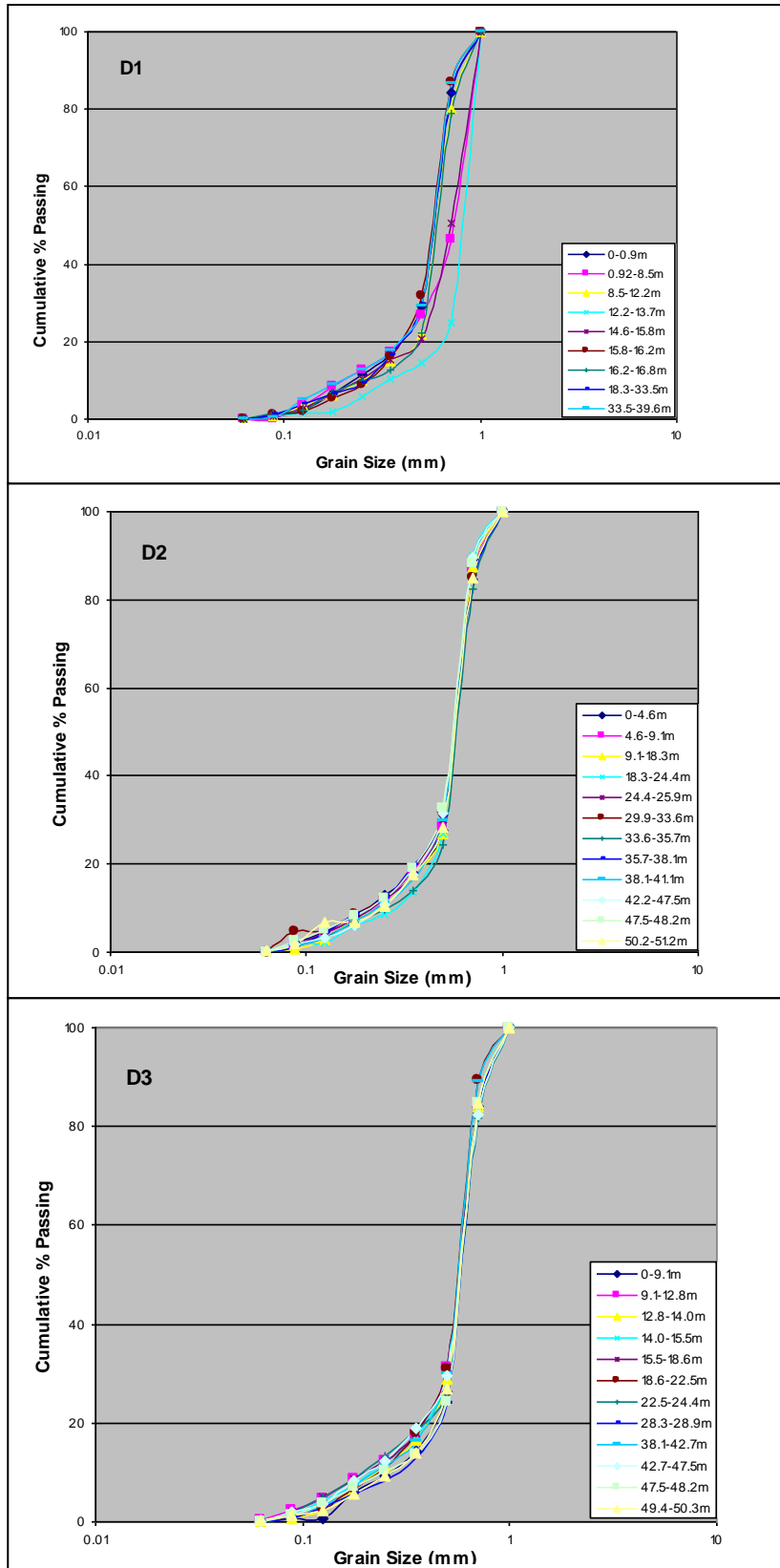
Figure 8.10a: Grading curves of samples falling within the paleochannel (see Figure 8.8 for locations).
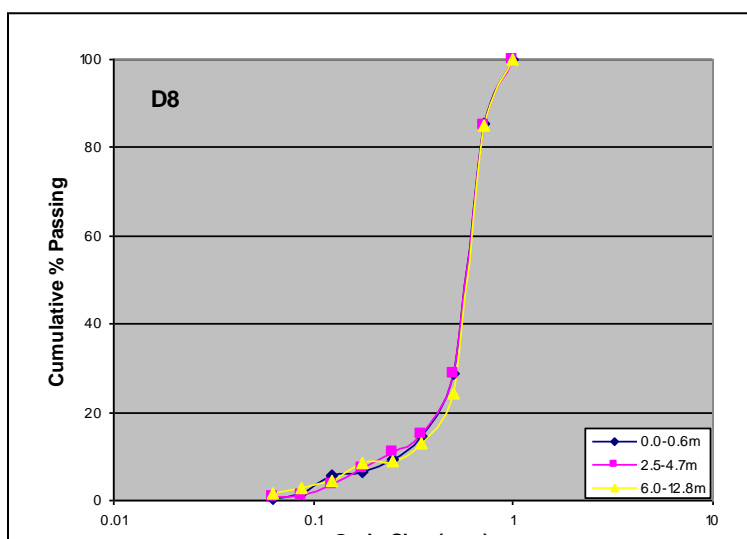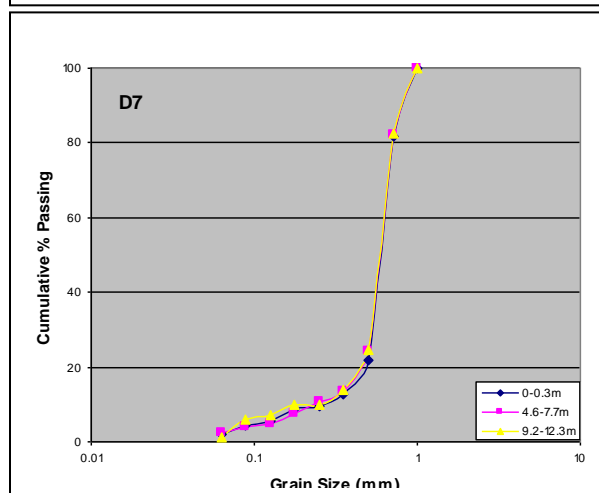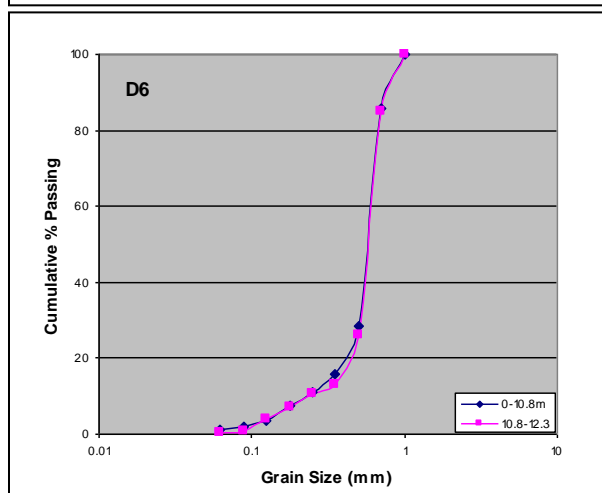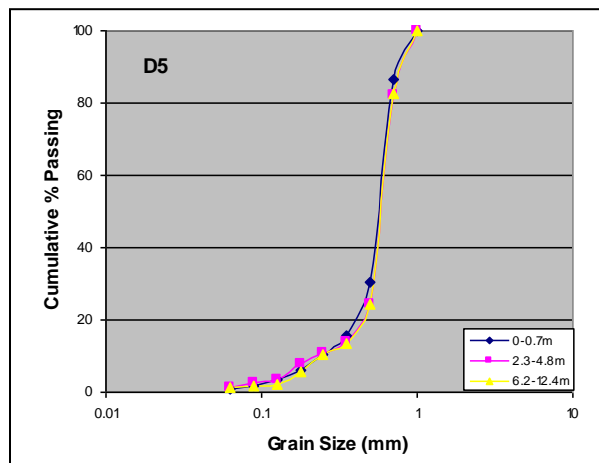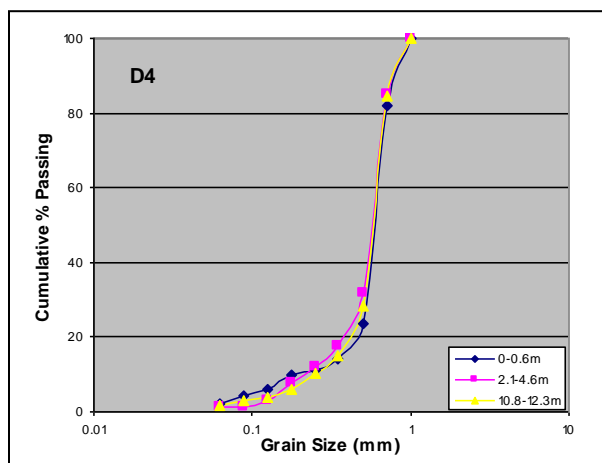
Figure 8.10b: Grading curves of samples falling within the paleochannel (see Figure 5.1 for locations).
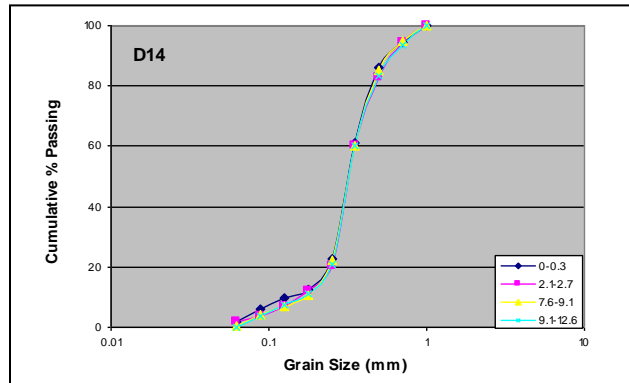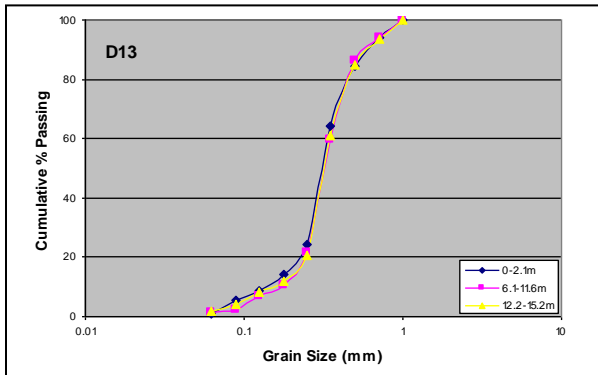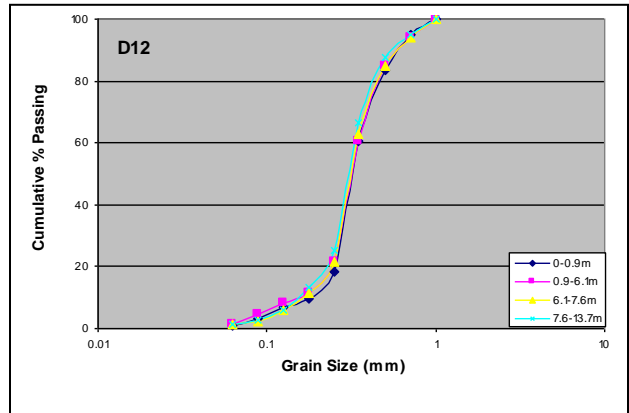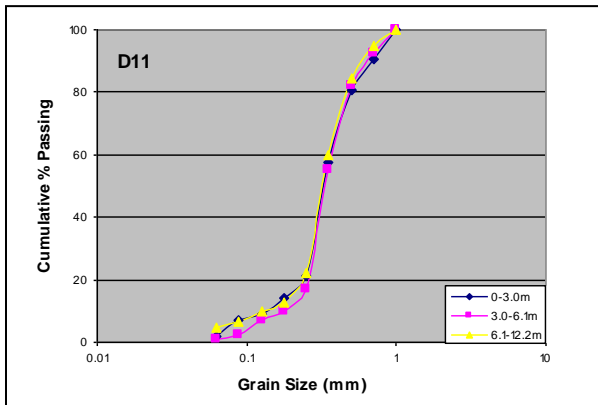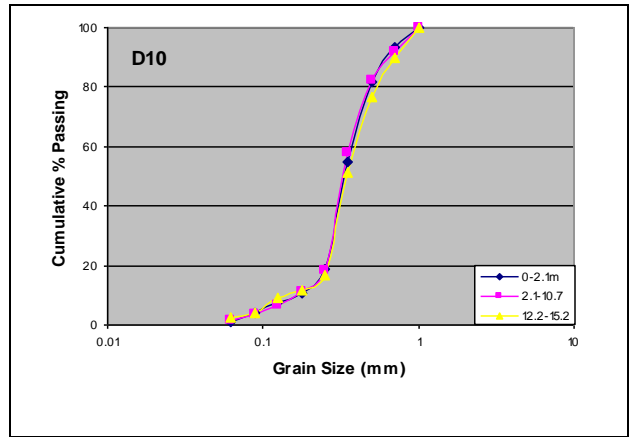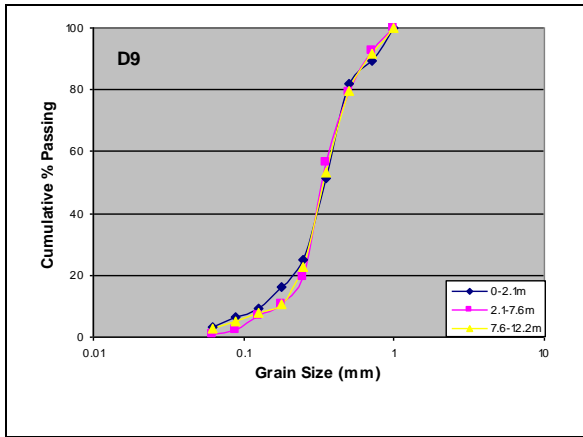
Figure 8.11a: Grading curves of samples falling within the alluvial plains (see Figure 5.1 for locations).
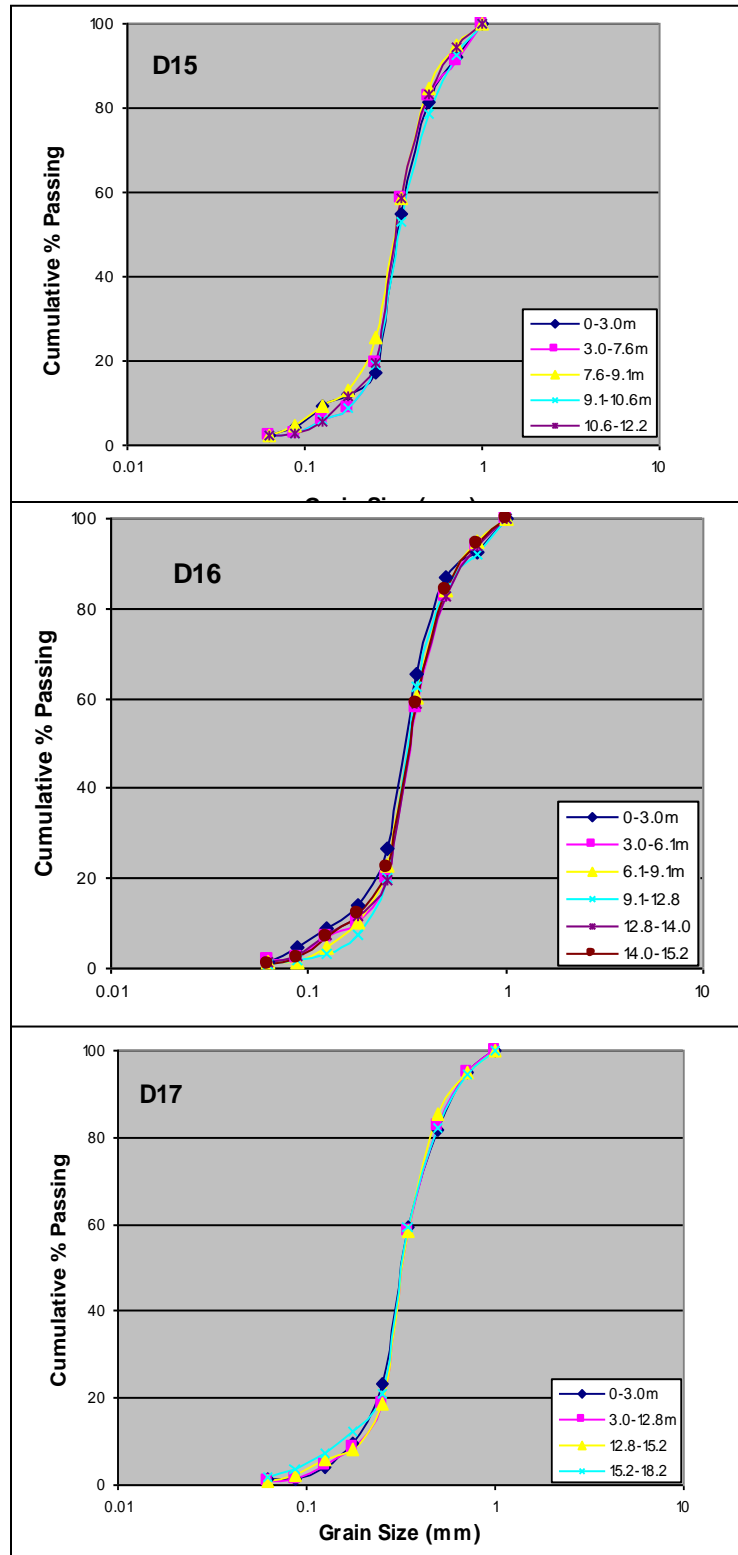
Figure 8.11b: Grading curves of samples falling within the alluvial plains (see Figure 5.1 for locations).
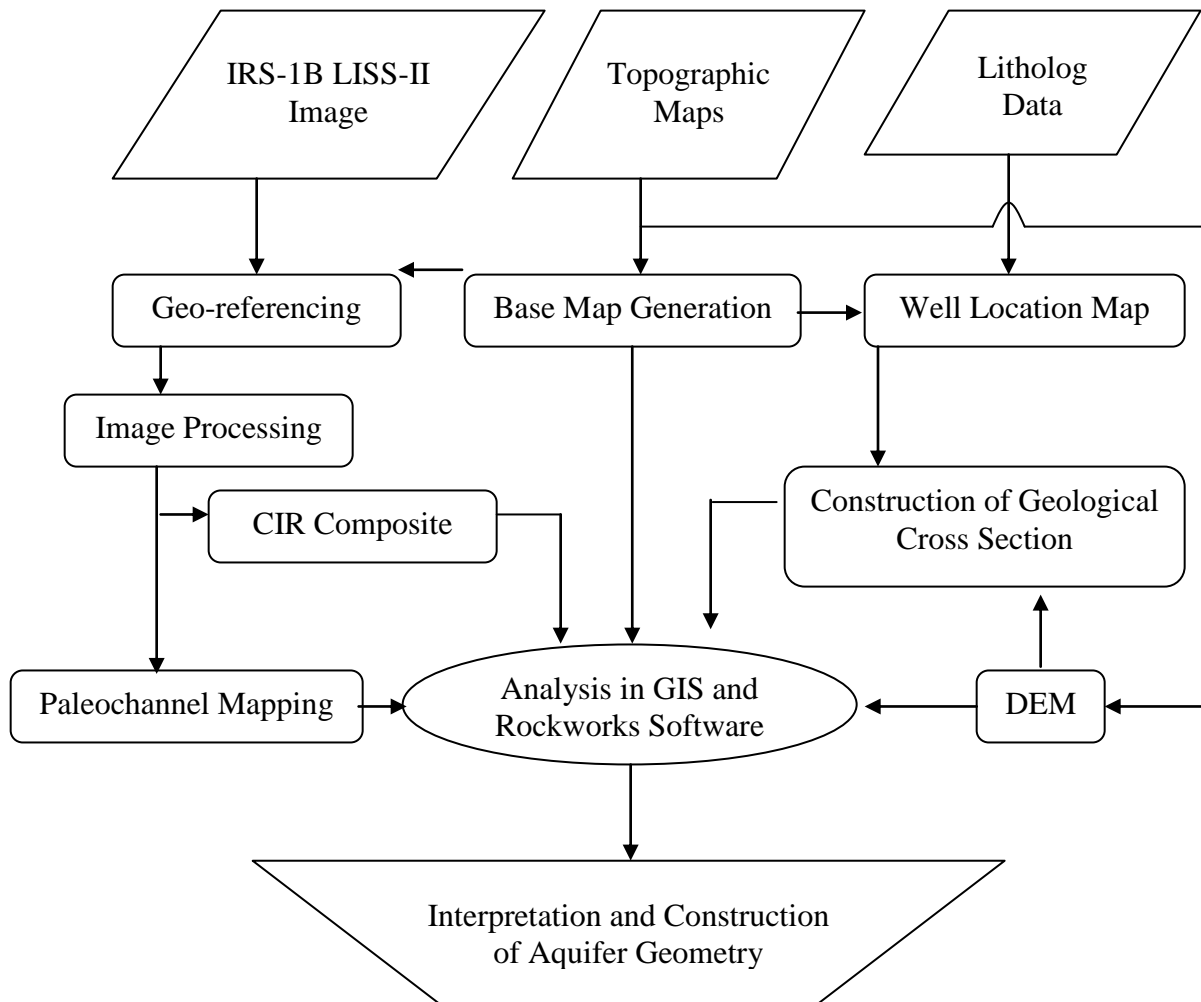
Figure 8.12: Flow diagram showing methodology for constructing aquifer geometry.
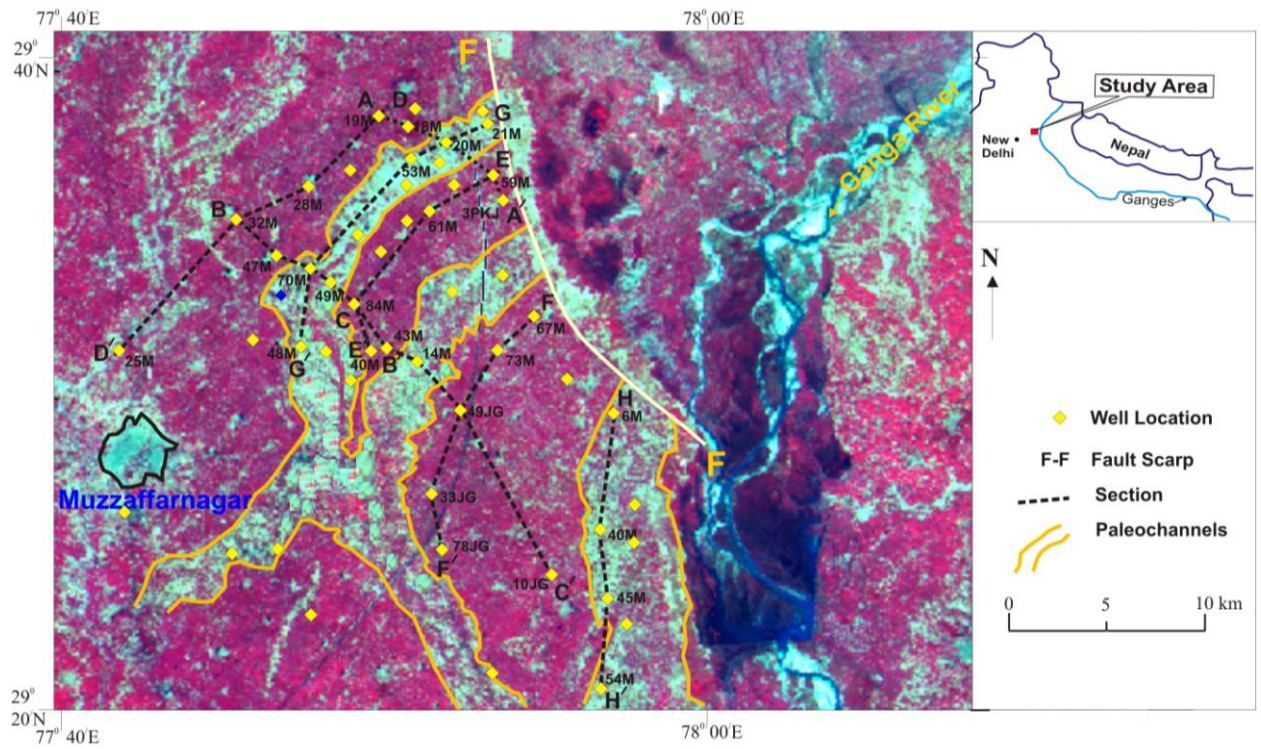
Figure 8.13: Well location marked on the Colour Infra-red Composite (R: NIR band; G: Red band; B: Green band), generated from the IRS-LISS-II (November, 1998) image data. Major locations, paleochannels and fault-scarp are also marked on the background.
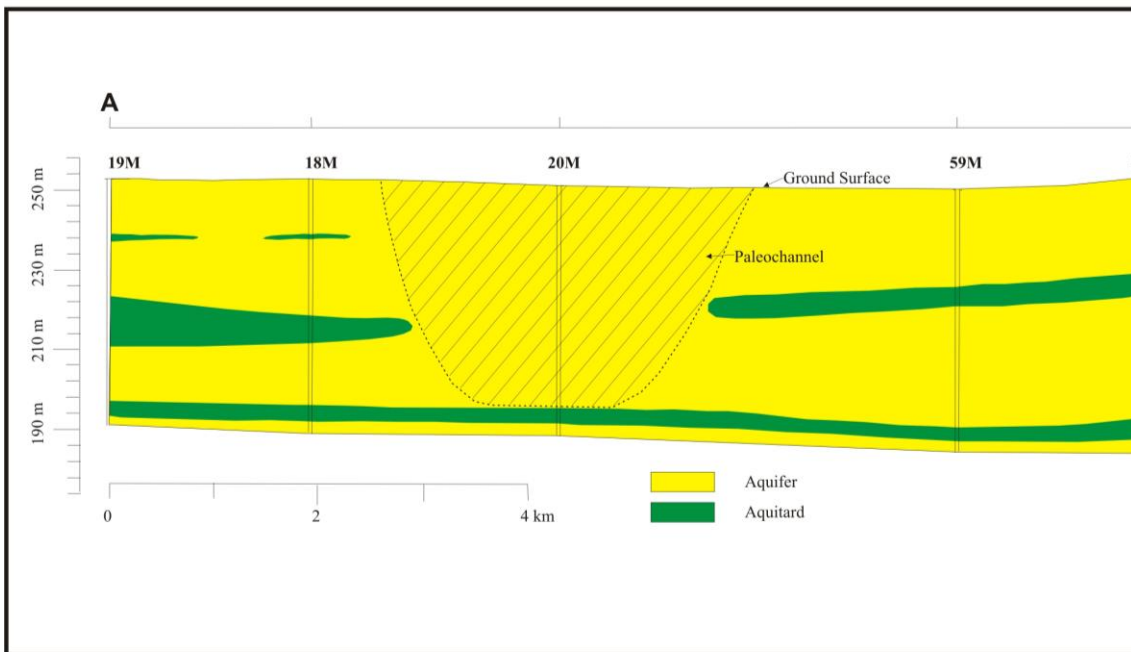
Figure 8.14: Interpreted geological section along A-A′ through well Nos. 19M, 18M, 20M, 59M and 3PKJ.
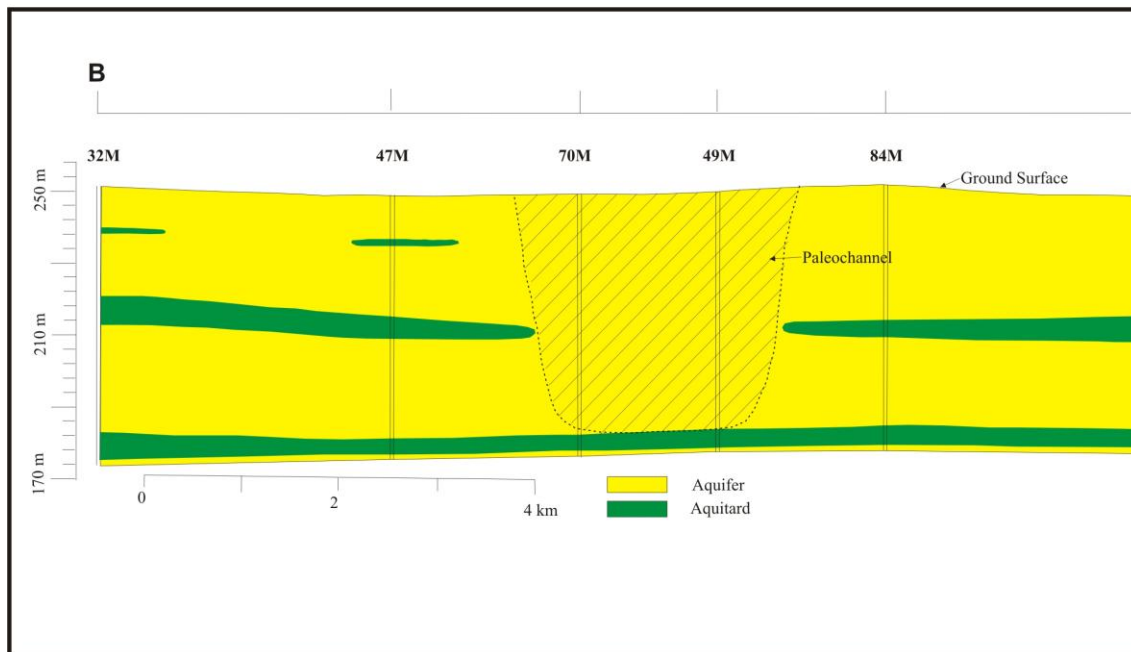
Figure 8.15: Interpreted geological section along B-B′ through well Nos. 32M, 47M, 70M, 49M, 84M and 43M.
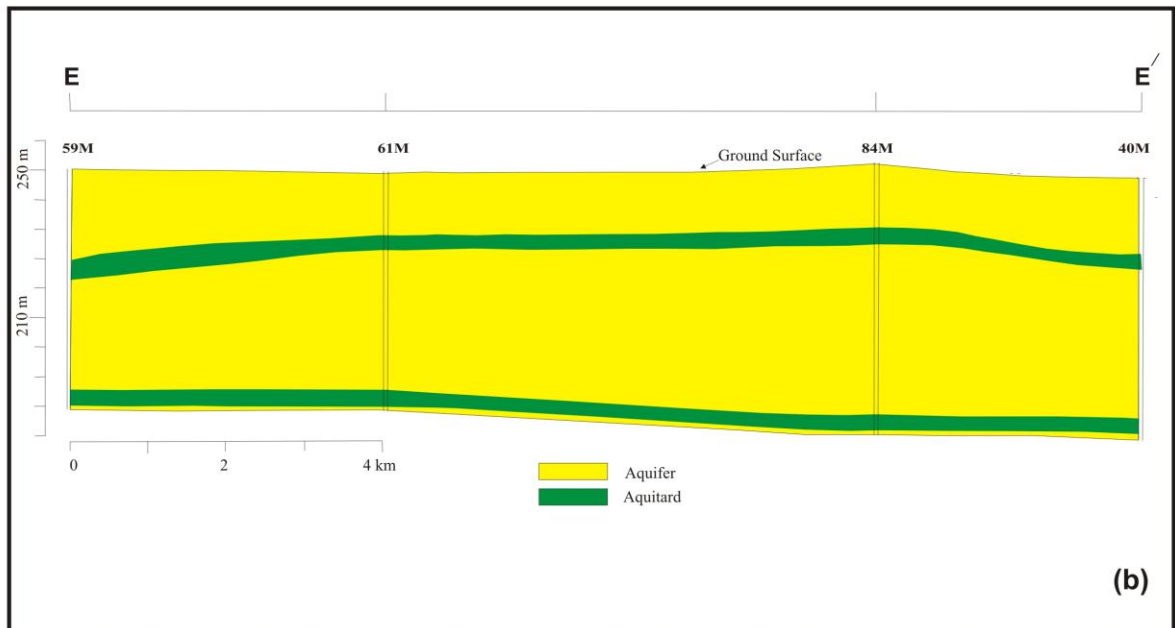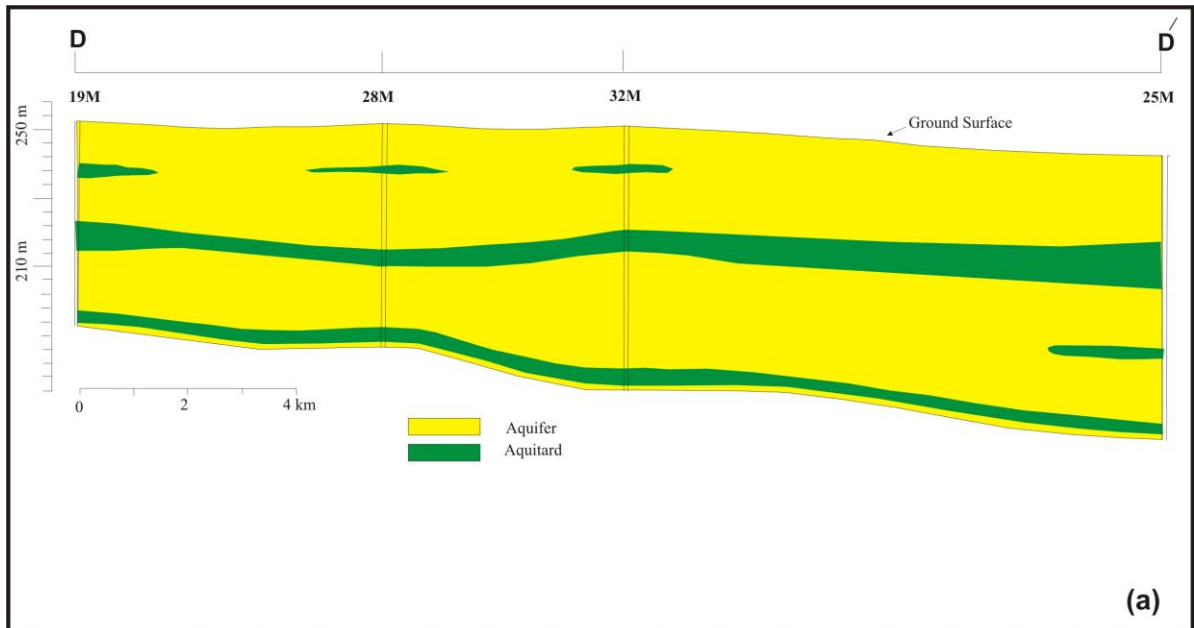
Figure 8.16: (a) Interpreted geological section along D-D′ through well Nos. 19M, 28M, 32M, and 25M. (b) Interpreted geological section along E-E′ through well Nos. 59M, 61M, 84M and 40M. Line of section and well locations are shown in Figure 8.13.
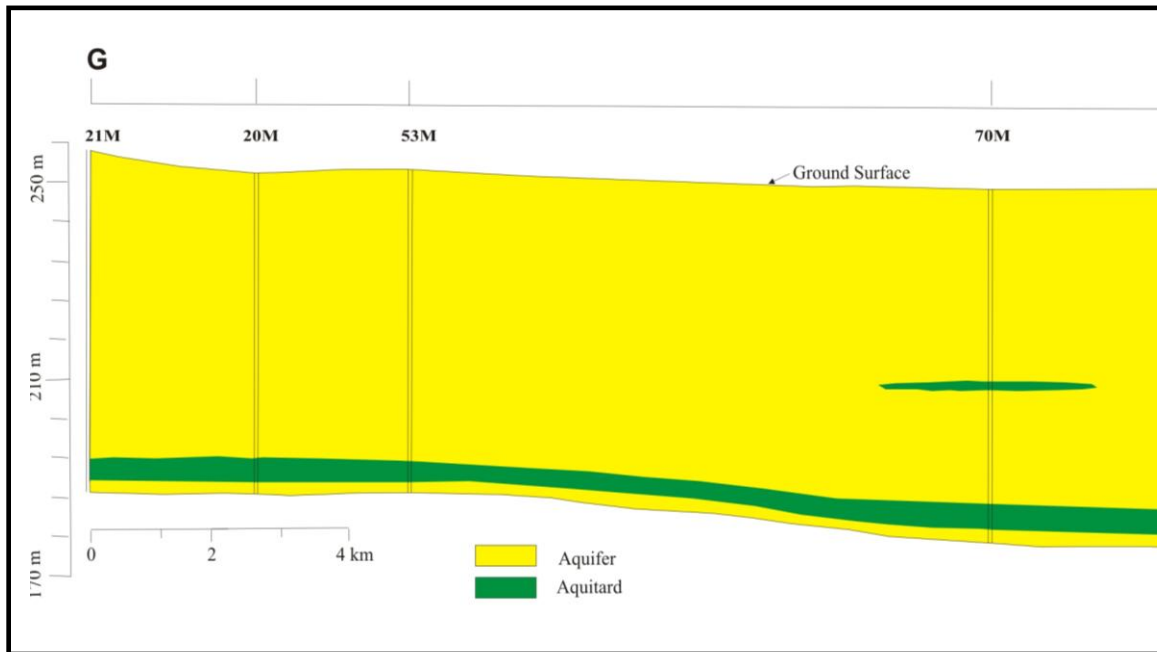
Figure 8.17: Interpreted geological section along G-G′ through well Nos. 21M, 20M, 53M, 70M and 49M.
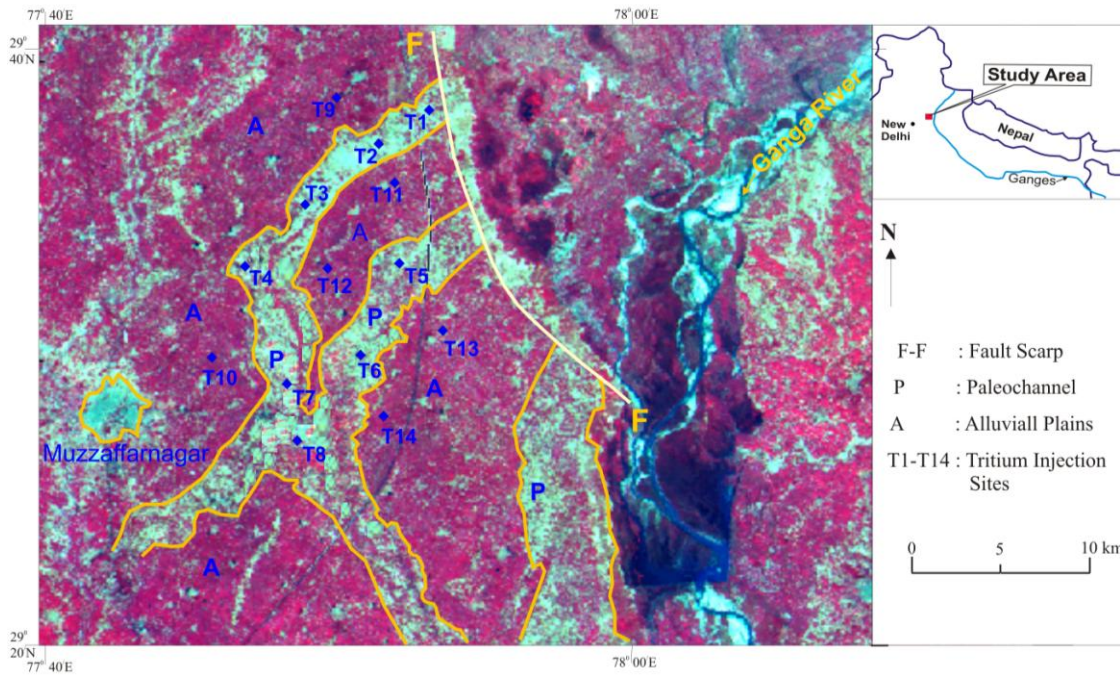
Figure 8.18: Location of tritium injection sites in paleochannels and alluvial plains, marked on the colour infra-red composite of IRS-LISS-II image data (NIR band coded in red colour; Red band coded in green colour; and Green band coded in blue colour).
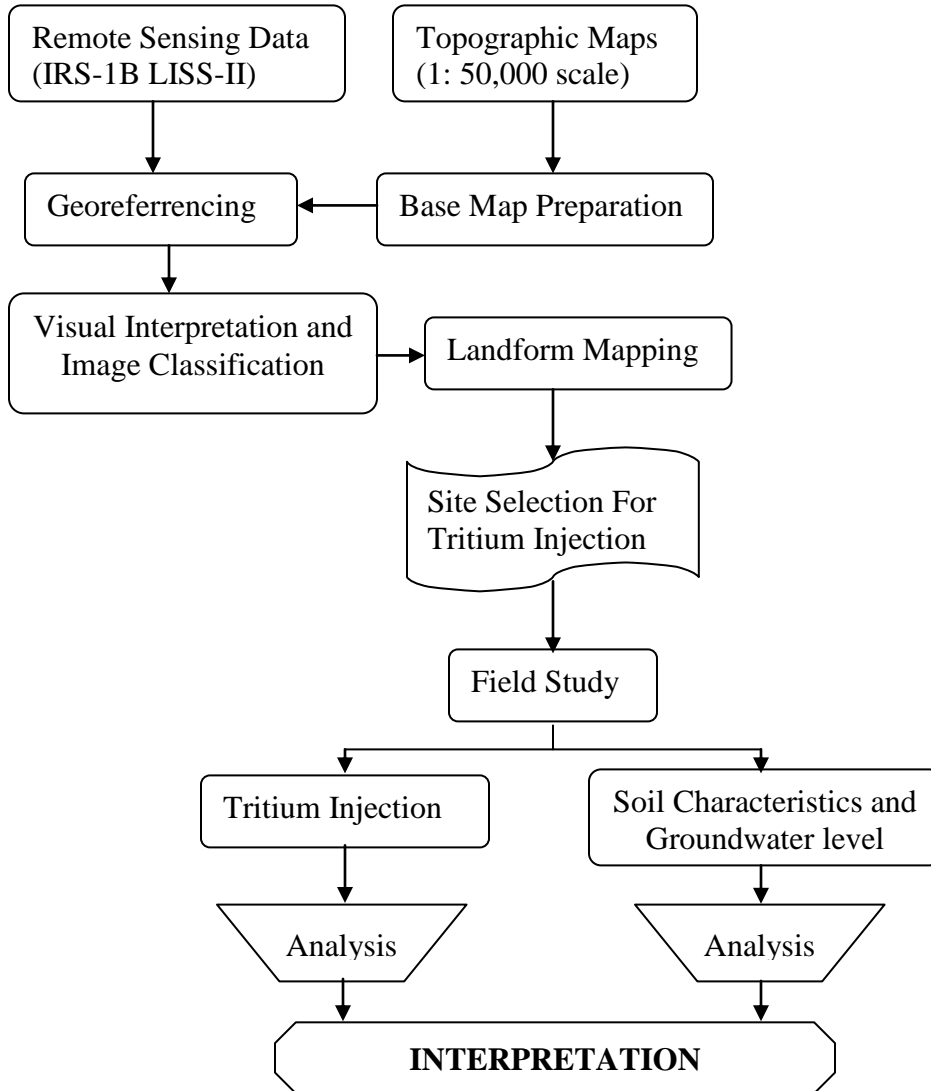
Figure 8.19: Flow diagram showing methodology adopted for estimating natural groundwater recharge using tritium tagging technique.
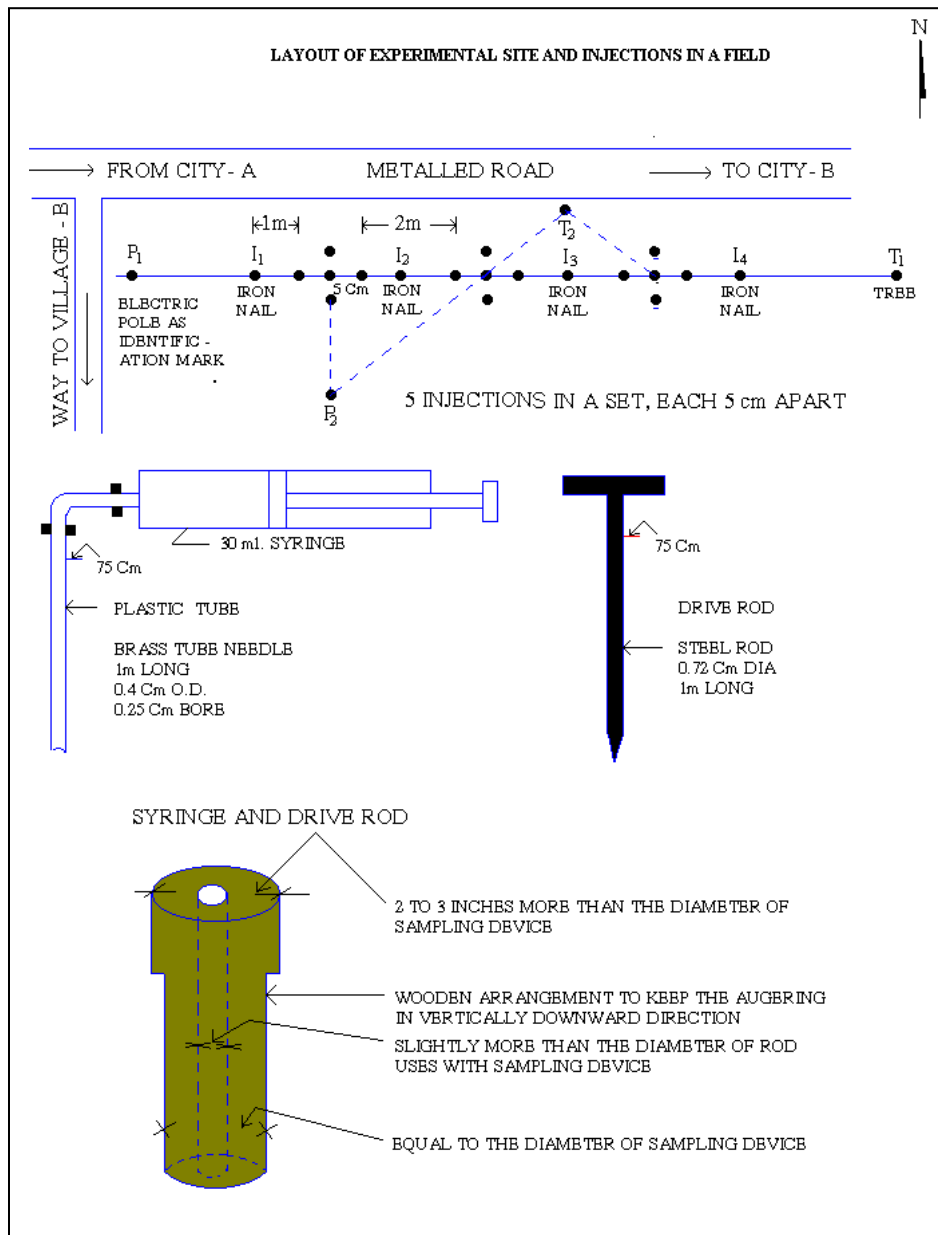
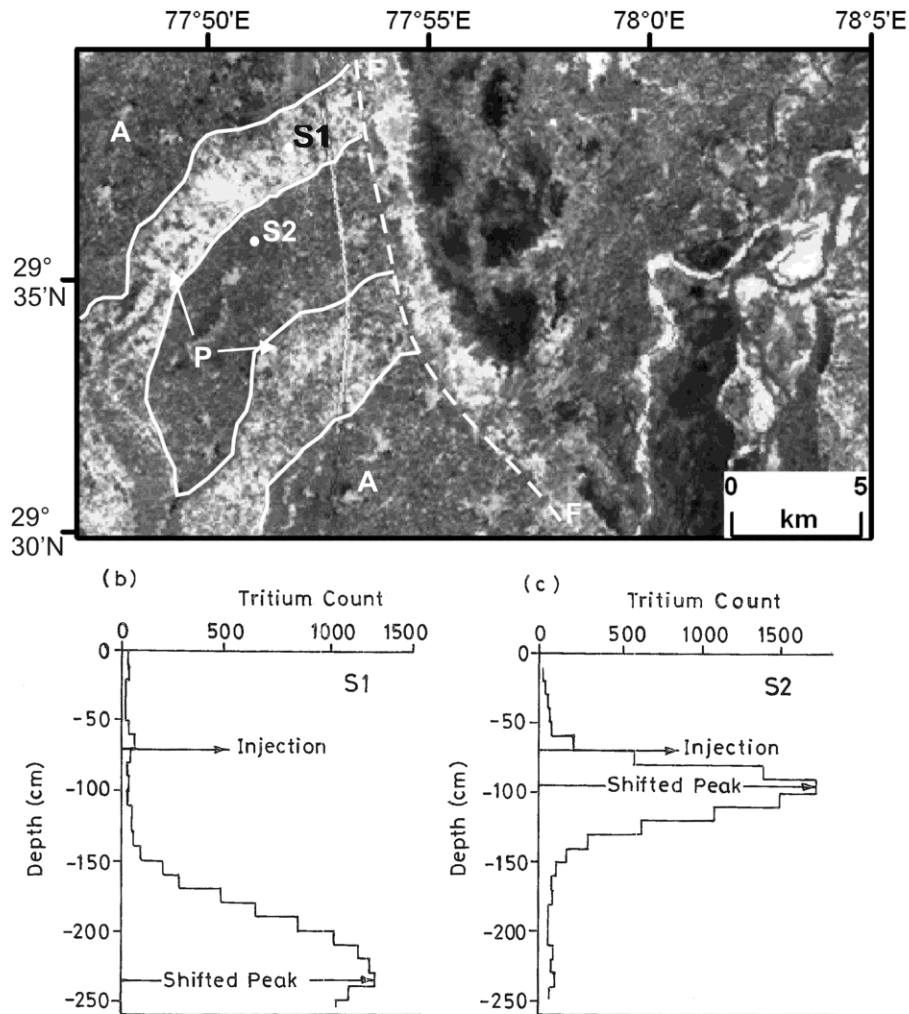**Figure 8.20: Systematic diagram of injection layout for artificial tritium injection at test sites (NIH).**
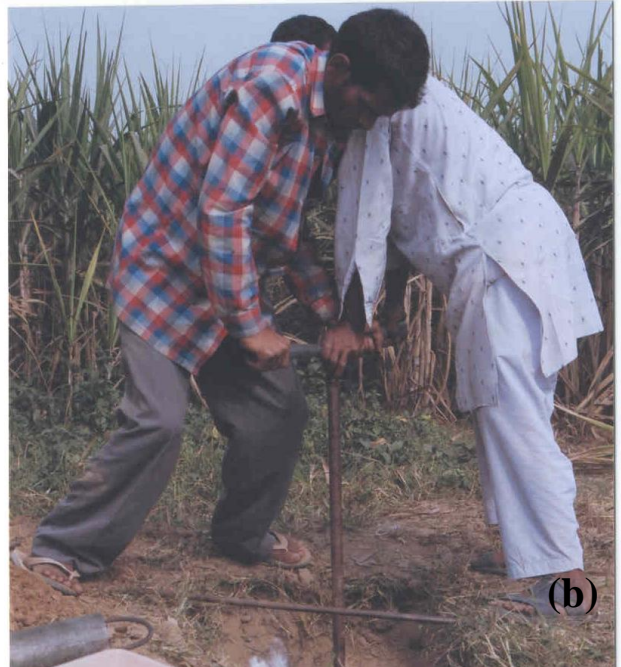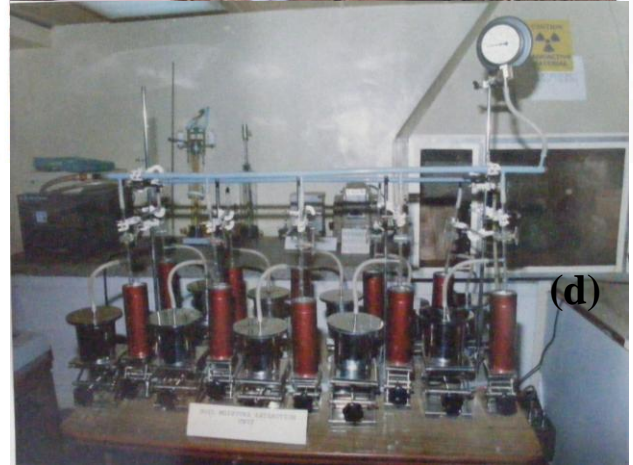
Figure 8.21: (a) Tritium injection at selected site.
      (b) Soil sampling during field investigation.
      (c) Liquid scintillation counter at NIH (Model: WALLAC 1409).
   **(d) Soil moisture extraction set up.**

Figure 8.22: Estimation of groundwater recharge by monitoring vertical movement of injected tritium. *a* shows an IRS-LISS-III image; injection of tritium was carried out at site *S1* in the paleochannel and at *S2* in the adjacent alluvial plain. Injection was uniformly made at 70 cm depth below ground level at pre-monsoon time. After monsoon, the tritium peak was found to have shifted by 160 cm in the paleochannel area, and by 40 cm in the alluvial plains (*Fig. b*).
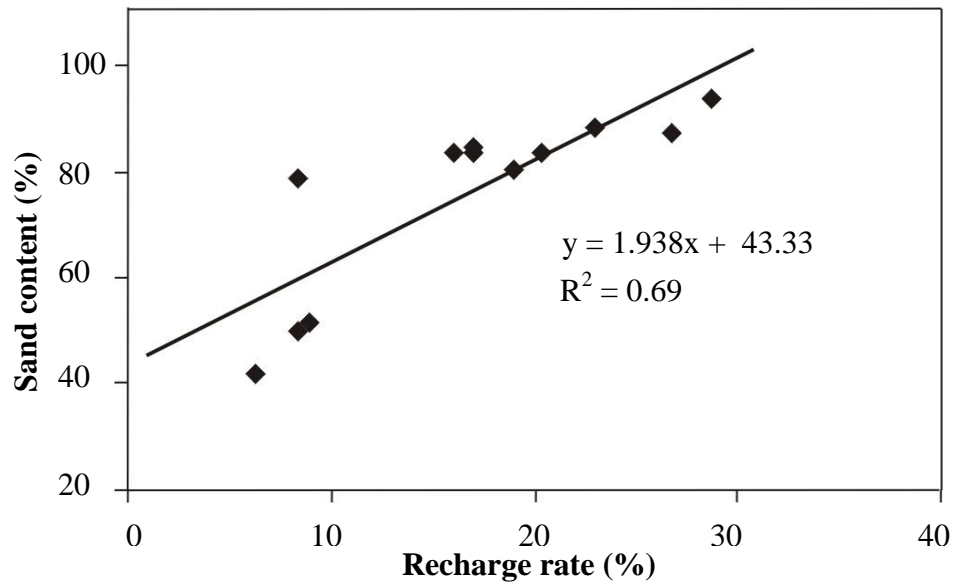
Figure 8.23: Relationship between average sand content (%) and corresponding recharge rate (%).
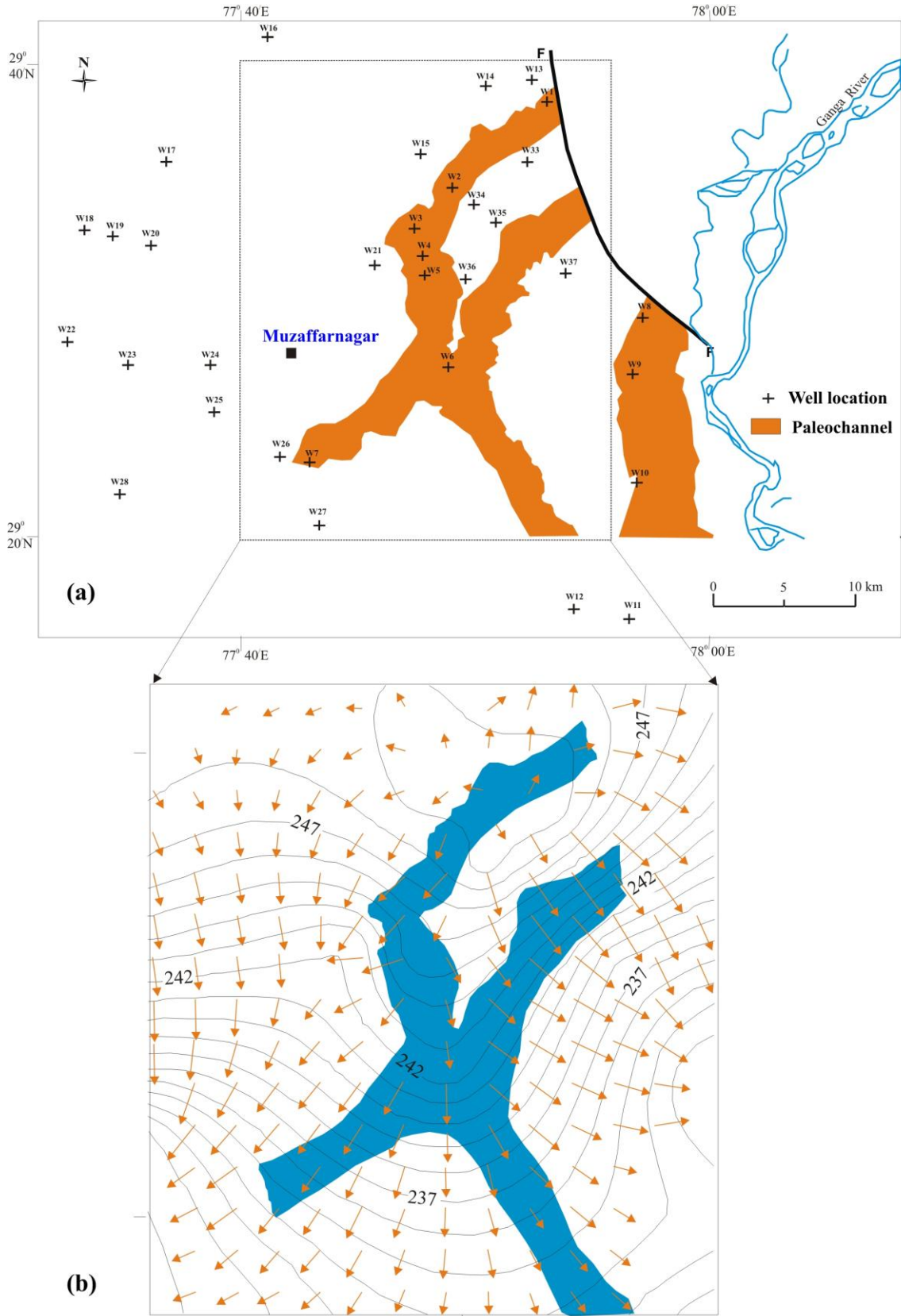
Figure 8.24: **(a) Location map of wells; (b) Pre-monsoon reduced groundwater level contour and flow direction map.**
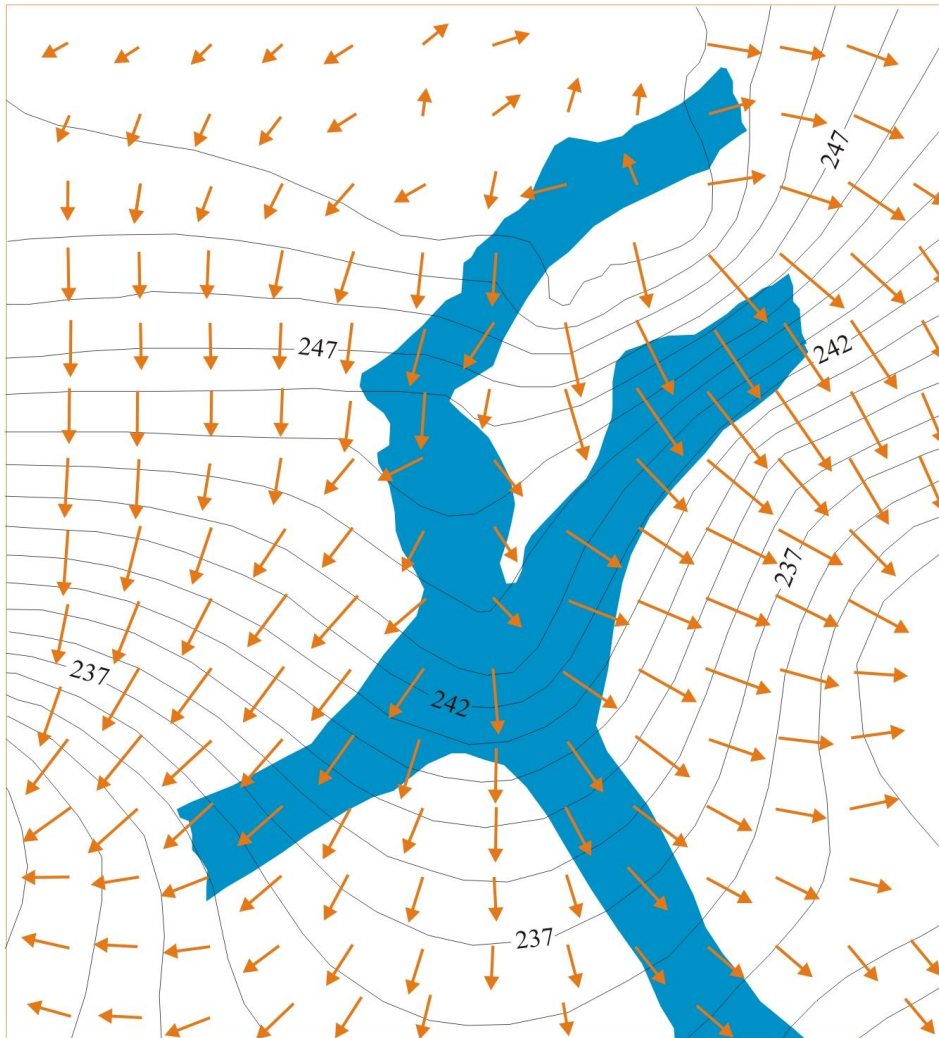
Figure 8.25: **Post-monsoon reduced groundwater level contour and flow direction map.**